Localization of the interaction site of herpes simplex virus glycoprotein D (gD) on the membrane fusion regulator, gH/gL

Tina M. Cairns[1*], Doina Atanasiu[1], Wan Ting Saw[1], Huan Lou[1], J. Charles Whitbeck[1], Noah T. Ditto[3], Birgitte Bruun[4], Helena Browne[4], Lucas Bennett[5], Chun Wu[5,6], Claude Krummenacher[5,7], Benjamin D. Brooks[8], Roselyn J. Eisenberg[2**], and Gary H. Cohen[1]

[1]Department of Basic and Translational Science, School of Dental Medicine, [2]Department of Pathobiology, School of Veterinary Medicine, University of Pennsylvania, Philadelphia, PA, USA

[3]Carterra Inc., Salt Lake City, UT, USA

[4]Division of Virology, Department of Pathology, University of Cambridge, Cambridge, UK

[5]Department of Molecular and Cellular Biosciences, [6]Department of Chemistry and Biochemistry, [7]Department of Biological Sciences, Rowan University, Glassboro, NJ, USA

[8]Rocky Vista University, Ivins, UT, USA

*Corresponding author

E-mail: tmcairns@upenn.edu (TMC)

**deceased

Abstract

A cascade of protein-protein interactions between four herpes simplex virus (HSV) glycoproteins (gD, gH/gL, gB) drive fusion between the HSV envelope and host membrane, thereby allowing for virus entry and infection. Specifically, binding of gD to one of its receptors induces a conformational change that allows gD to bind to the regulatory complex gH/gL, which then activates the fusogen gB, resulting in membrane fusion. Using surface plasmon resonance and a panel of anti-gD monoclonal antibodies (MAbs) that sterically blocked the interaction, we previously showed that gH/gL binds directly to gD at sites distinct from the gD receptor binding site. Here, using an analogous strategy, we first evaluated the ability of a panel of uncharacterized anti-gH/gL MAbs to block binding to gD and/or inhibit fusion. We found that the epitopes of four gD-gH/gL blocking MAbs were located within flexible regions of the gH N-terminus and the gL C-terminus, while the fifth was placed around gL residue 77. Taken together, our data localized the gD binding region on gH/gL to a group of gH and gL residues at the membrane distal region of the heterodimer. Surprisingly, a second set of MAbs did not block gD-gH/gL binding but instead stabilized the complex by altering the kinetic binding. However, despite this prolonged gD-gH/gL interaction, "stabilizing" MAbs also inhibited cell-cell fusion, suggesting a unique mechanism by which the fusion process is halted. Our findings support targeting the gD-gH/gL interaction to prevent fusion in both therapeutic and vaccine strategies against HSV.

Importance

Key to developing a human HSV vaccine is an understanding of the virion glycoproteins involved in entry. HSV employs multiple glycoproteins for attachment, receptor interaction, and

membrane fusion. Determining how these proteins function was resolved, in part, by structural biology coupled with immunological and biologic evidence. After binding, virion gD interacts with receptor, activates the regulator gH/gL complex, triggering gB to drive fusion. Multiple questions remain, one being the physical location of each glycoprotein interaction site. Using protective antibodies with known epitopes, we documented the long-sought interaction between gD and gH/gL, detailing the region on gD important to create the gD-gH/gL triplex. Now, we identified the corresponding gD contact sites on gH/gL. Concurrently we discovered a novel mechanism whereby gH/gL antibodies stabilize the complex and inhibit fusion progression. Our model for the gD-gH/gL triplex provides a new framework for studying fusion which identifies targets for vaccine development.

Introduction

The entry of herpes simplex virus (HSV) into a mammalian cell requires the coordinated action of four viral glycoproteins (gD, gH/gL, gB). However, unlike many other viruses, herpesviruses encode receptor-binding and membrane fusion functions on separate proteins (gD and gB, respectively). As such, fusion is driven by a cascade of protein-protein interactions that is initiated by the binding of gD to one of its cellular receptors (HVEM or nectin-1) (1-7).

HSV gH is a type I transmembrane protein, whereas HSV gL is not membrane-anchored and associates non-covalently with the gH ectodomain. On mature virions and on the surface of HSV-infected cells, gH and gL are found together in a stable 1:1 heterodimeric complex (8). The crystal structure of a modified form of HSV-2 gH/gL revealed an extensive interaction between

the two proteins that explained their interdependence for folding, transport, and function (8-11). gH/gL work together as a unit to regulate the activity of the herpesvirus fusogen, gB (1, 9, 12-14). However, the activity of gH/gL itself is regulated by another viral protein, gD (1, 13, 15).

Crystal structures of gD with and without HVEM or nectin-1 (16-19) reveal that the C-terminus of the gD ectodomain normally occludes the receptor binding site and must move away before it can interact with the receptor. We hypothesize that this conformational change in gD also promotes its physical interaction with gH/gL, thereby resulting in its functional activation and consequent promotion of the cascade of events leading to fusion (1, 12). A form of HSV gH/gL containing only the heterodimer ectodomain can trigger fusion of cells expressing gB, gD, and a gD receptor (albeit with lower efficiency than full-length gH/gL) (1), suggesting that the postulated physical interaction between gD and gH/gL occurs within the gH/gL ectodomain. Furthermore, by generating gH/gL chimeras encoding segments of HSV-1 and saimiriine herpesvirus-1 sequence, a gD interaction site on gH/gL was roughly mapped to the N-terminal half of the gH ectodomain (20).

In our previous study, we used surface plasmon resonance (SPR) to demonstrate binding between soluble forms of HSV-2 gD (gD2) and gH/gL (gH2/gL2) (21). We used a form of gD [gD2(285t)] with the C-terminus removed (22), so it would already be "primed" for interaction with gH/gL (23). The soluble gD was captured to a biosensor chip via an anti-gD monoclonal antibody (MAb) that presented the gH/gL binding face of gD, and then soluble gH/gL was added. We found that gH/gL bound directly to gD with a relatively fast on- and off-rates. Anti-gD MAbs were identified that blocked the binding of gH/gL and the detailed location of their epitopes outlined a potential gH/gL binding region on gD that spanned a face adjacent to, but distinct from, the nectin-1 and HVEM binding sites.

Having identified the gH/gL binding site on gD, we next set out to determine the physical location of the reciprocal binding site on gH/gL. To accomplish this, we first characterized a panel of anti-gH/gL MAbs and grouped them into antigenic communities sharing similar competitive traits. We then determined their ability to block the interaction of gD-gH/gL and assessed their function in a cell-cell fusion assay. The MAbs separated into three groups: 1) those that had no effect on either gD-gH/gL binding or cell-cell fusion; 2) those that blocked gD-gH/gL binding and inhibited cell-cell fusion; and 3) those that, surprisingly, stabilized the gD-gH/gL complex, a subset of which inhibited cell-cell fusion. By comparing the kinetics between gH/gL bound with IgG (dimeric binding) vs Fab (monomeric binding), we determined that the stabilization effect was due to the valence of IgG. However, valence had no impact on blocking gH/gL binding to gD, as both IgG and Fabs blocked equally well. Several of the MAbs that blocked the gD-gH/gL interaction localized to regions of gH/gL that were missing in the crystal structure; therefore, to visualize this potential binding region we developed a 3D structural model for the entire gH/gL ectodomain. We concluded that the gD binding region on gH/gL includes the very N-terminus of gH, the C-terminus of gL, and is centered around gL residue 77.

Results

Previously, we used a large panel of anti-gD MAbs (24) to screen for those that blocked gD-gH/gL binding, enabling us to determine a possible gH/gL binding region on gD (21). Here, we used a similar method to probe the corresponding side of the gD-gH/gL complex. For this, we first characterized a large panel of anti-gH/gL MAbs, and then screened them for their ability to block complex formation with gD. We hypothesized that the epitopes of anti-gH/gL MAbs that block binding to gD would locate a potential gD binding site on gH/gL. Furthermore, we

screened these MAbs for inhibition of fusion, theorizing that those that blocked gD-gH/gL binding would also have a functional impact.

For this study, we first used a high-throughput surface plasmon resonance (SPR) technique (24-26) to determine which of a panel of 36 MAbs compete for binding to gH/gL (Fig. 1A). First, MAbs (IgG) were covalently arrayed on an SPR sensor chip. Second, soluble gH/gL was injected across the chip surface followed by each of the 36 MAbs injected in series (26). Since our panel of MAbs contained both type-specific (bind either HSV-1 or HSV-2) and type-common (bind both HSV-1 and HSV-2), all MAbs were tested against both gH1/gL1 and gH2/gL2. Sensorgrams of the binding were analyzed to generate a heat map and dendrogram for each gH/gL protein (Fig. 1B-E). MAbs were arranged into bins to reflect competition vs. no competition (25-27), and grouped into a network plot, descriptive of which epitopes are engaged. The result is a graphical representation of the heat map (Fig. 1B, D). Finally, the data were depicted as MAb "communities" that reflect their competitive behavior (Fig. 2).

The MAb community maps for gH1/gL1 and gH2/gL2 are shown in Fig. 2A and 2B, respectively. We color-coded each community: purple, green, orange, blue, and yellow for gH1/gL1 (Fig. 2A) and purple, green, yellow, cyan, and red for gH2/gL2 (Fig 2B). The purple community of gH2/gL2 was further sub-divided into purple, orange, and magenta based on competition and previous mapping data (28). The arrangement of the MAbs within and between communities reflects the extent of competition. For example, the red community in gH2/gL2 form a tight, overlapping cluster of MAbs that have a high degree of competition between all members (Fig. 2B).

Here, we provided the first analysis of cross-competition between MAbs that bind specifically to either gH or gL, as our previous study examined anti-gH and anti-gL MAbs separately (28). Thus, this study allowed us to examine the relationships of MAbs in the gH/gL complex itself. Interestingly, the three MAbs against gL (28-30) were sorted into their own communities (CHL18 to the cyan community of gH2/gL2 and L4 and CΔ48L3 to the yellow communities of gH1/gL1 and gH2/gL2, respectively).

Epitope mapping MAbs that bind gH2/gL2.

Our next objective was to map the epitopes of key members of each community and position them onto the 3D structure of gH2/gL2. To account for residues that were not resolved by crystallography (9), we used a hypothetical model of the complete gH2/gL2 ectodomain (Fig. 3). Previous peptide binding data (28, 31) localizes the epitopes of yellow (CΔ48L3), cyan (CHL18), magenta (CHL17, CHL32), and orange (CHL29, CHL30, CHL31, CHL35) MAbs to specific stretches of amino acids (gL 173-183, gL 208-219, gH 19-38, gH 145-155 and 676-686, correspondingly) (Fig. 4). Likewise, monoclonal antibody resistant (*mar*) virus data for CHL2 localizes the red community around gH residue 116 (28). However, we had no information regarding the location of the purple (CHL21, CHL37) and green (CHL27, 53S) communities. Only 6 of the 36 anti-gH/gL MAbs bind type-common epitopes, i.e. bind both gH1/gL1 and gH2/gL2 (designated by asterisks in Fig. 2A, B). The type-common MAbs, which are found in purple, orange, and green communities, serve as a "bridge" between data generated on either gH1/gL1 or gH2/gL2 through the type-specific MAbs with which they compete.

(i) Epitope mapping of CHL21 and CHL37.

159 CHL21 and CHL37 (purple community) recognized type-common epitopes, but also
160 competed with type-1 specific MAbs 46S, 52S, and BBH5 (Fig. 2A). CHL37 was previously
161 characterized via Western blot analysis as a linear, type-2 specific anti-gH MAb (28). Here, we
162 show that newly characterized MAb CHL21 behaves in a similar fashion by Western blot (Fig.
163 5A). In contrast to the Western data, both CHL37 and CHL21 bind to gH1/gL1 via SPR (Fig.
164 5B), suggesting that the epitopes of CHL21 and CHL37 in gH1/gL1 are more sensitive to the
165 detergent used in both denaturing and "native" Western blot analyses (32). We previously used a
166 panel of overlapping peptides to localize CHL37 to the N-terminus of gH (28). However, we
167 found that it (and CHL21) can bind to gH2Δ48/gL2 (Fig. 5A, B), which contains an N-terminal
168 gH deletion, suggesting that its epitope lies further downstream. This discrepancy may be due to
169 amino acid similarity between the N-terminus of gH and the CHL37 epitope. Based on
170 competition with 52S (33) and BBH5 (Materials and Methods) (Fig. 2A), we placed the epitopes
171 of CHL21 and CHL37 within the C-terminal half of gH, where the 52S epitope has been located
172 (Fig. 4).

173 *(ii) Epitope mapping of CHL27.*

174 To determine the location of the CHL27 epitope, we used SPR to screen for binding to
175 several forms of gH/gL (Fig. 6A). CHL27 bound to both gH1/gL1 and gH2/gL2 but was unable
176 to bind to gH2Δ48/gL2 (Fig. 6A), indicating that its epitope lies within the gH2 N-terminus.
177 Interestingly, MAb 53S, which competes with CHL27 for binding to gH/gL (Fig. 2A, B), bound
178 to gH2Δ48/gL2 (Fig. 6A), effectively separating the location of these two MAb epitopes.

179 We next screened CHL27 for binding to gH peptides, particularly those within the N-
180 terminal region. CHL27 bound to two gH2 peptides, one comprising residues 28-47 and the

other comprising residues 37-56 (Fig. 6B), thus defining its epitope to within amino acids 37-47 (Fig. 4; Fig. 6C). We used Western blot analysis of five full-length gH point mutants (previously characterized in Cairns et al. (34)) to confirm the peptide data. Four mutations (R39A, Y41A, R43A, D44A) abrogated CHL27 binding (Fig. 6D). Therefore, we conclude that the epitope for CHL27 encompasses at least these four residues within the gH N-terminus (Fig. 6C, green).

(iii) Epitope mapping of 53S.

Prior studies suggest that the conformation-dependent epitope of 53S is located in the N-terminal half of gH/gL and may contain gL residues (8, 35-39). 53S competes with CHL27 for gH/gL binding (Fig. 2A B) yet these two MAbs bind to distinct regions of gH/gL, as removal of the gH N-terminus abrogates CHL27 binding but not 53S binding (Fig. 6A). To localize the 53S epitope, we combined our Carterra (Fig. 1) and BIACORE (data not shown) SPR competition data to develop a 53S "competition tree" showing its relationships with other MAbs (Fig. 7A). 53S competes for binding with CHL27, BBH3, and LP11, but not with BBH2 or BBH4. Interestingly, 53S and LP11 exhibited unidirectional competition, as inhibition was dependent on which MAb bound to gH/gL first; if LP11 bound first, binding of 53S was blocked but not vice versa. This result suggests that either a conformational change occurs upon binding of LP11 that prevents 53S from binding, or that binding of LP11 prevents a conformational change required for 53S to bind. BBH2 and BBH4, which compete with LP11, do not compete with 53S or CHL27 (Figs. 2A). Using point mutations in gH1 known to abrogate the binding of these five MAbs (LP11, CHL27, BBH3, BBH2/BBH4) as a guide, we localized a potential region for the 53S epitope on gH2: "north" of LP11, "east" of BBH3, and "west" of CHL27 in the 3D model (Fig. 7B, dotted circle). Two previously characterized gL insertion mutants which show a decreased reactivity to 53S (P48 and R55) also lie in this region (39).

204 To further define the 53S epitope we chose nine surface-accessible amino acids [two gH
205 residues (V161, T162) and seven gL residues (R46, D50, D51, P77, Q138, H142, P144)] to
206 mutate to alanine and test for 53S binding (Fig. 7B, green). Each mutation was placed into a
207 mammalian expression plasmid containing full-length gH2. The two mutant forms of gH2 and
208 seven of gL2 were co-transfected into C10 cells with WT-gL2 or gH2, respectively. Total cell
209 lysates were tested for protein expression by reactivity to anti-gH2/gL2 polyclonal antibody
210 (PAb) R176 using Western blotting (Fig. 7C). Although all proteins were expressed, mutant gH-
211 V161A was present at reduced levels and contained a lower level of glycosylated gH (the top
212 band of the gH doublet, Fig. 7C), indicative of altered protein processing and insufficient
213 trafficking to the cell surface (10, 11, 34). However, with the exception of gH-V161A, all
214 mutants had near-WT levels of cell-surface expression as detected by MAbs CHL27 (anti-gH)
215 and CΔ48L3 (anti-gL) in a CELISA (Fig. 7D).

216 Due to 53S binding a conformational epitope (and being unreactive in Western blotting
217 due to the presence of detergent), 53S reactivity was examined by CELISA. Only mutant gL-
218 P77A was severely deficient in 53S binding (Fig. 7C). This reduction in 53S binding was not
219 indicative of poor processing or lack of cell-surface protein expression (Fig. 7C, D).

220 We next used the split luciferase (cell-cell) fusion assay (SLA) (29, 40) to test each
221 mutant for function. In the SLA, reconstitution of functional luciferase from its two "split"
222 domains, $Rluc8_{(1–7)}$ and $Rluc8_{(8-11)}$, individually expressed in effector and target cells, reflects the
223 level of fusion. Effector B78H1 cells were transfected with gB2, gH2, gL2 and $Rluc8_{(1–}$
224 $_{7)}$ plasmids, while target C10 cells expressing the gD receptor nectin-1 were transfected with
225 $Rluc8_{(8–11)}$ plasmid (41). Effector cells were incubated with the SLA substrate for 1 h before
226 target cells were added. Soluble gD2(306t) was added when effector and target cells were mixed

to trigger fusion and activity was measured for 2 h. As expected due to its reduced expression, mutant gH-V161A exhibited a 60% decrease in fusion activity as compared to WT gH (Fig. 7E). However, mutant gL-P77A was fully functional in cell-cell fusion (Fig. 7E). Thus, with its loss of 53S binding but retention of fusion function, mutant gL-P77A appeared to resemble a 53S MAb-resistant (*mar*) mutant protein (42).

Anti-gH/gL MAbs block or stabilize gD-gH/gL binding.

In our previously described SPR assay (Fig. 8A), we detected an interaction between gD2 and gH2/gL2 when gD was captured by certain anti-gD MAbs and presented on a biosensor chip and gH/gL was flowed (i.e., gD is the ligand and gH/gL is the analyte) (Fig. 8B), but not in the reverse orientation (21). This interaction was prevented by the binding of a subset of anti-gD MAbs bound to gD prior to addition of gH/gL, enabling us to identify the gH/gL binding "face" on gD (21). Having defined the epitopes of our anti-gH/gL MAb panel, our next goal was to exploit this technique to define the site on gH/gL that interacts with gD.

We adapted this experimental design to map the gD binding site on gH/gL (Fig. 9A). In this approach, we first incubated gH/gL with anti-gH/gL MAbs for 10 minutes prior to injection across a chip containing gD captured by 1D3. The control was to flow gH/gL alone (Fig. 9, black curves). The colored curves show gH2/gL2 binding when pre-incubated with the indicated MAb, with each color signifying its community membership (Fig. 2B). Importantly, we found that a subset of anti-gH/gL MAbs blocked gD-gH/gL binding while others did not (Figs. 9B-E). MAbs in the green (53S, CHL27) and magenta (CHL17, CHL32) communities blocked the interaction with gD by 85-100%, and MAb CHL18 decreased gH/gL binding to gD by 50% (Fig. 9B). In contrast, MAbs in the orange community had no effect on gD-gH/gL binding (Fig. 9C).

We also found a third, unexpected, outcome. When MAbs from the purple (CHL21, CHL37), red (CHL2, CHL4) or yellow (CΔ48L3) communities were pre-incubated with gH/gL, binding to gD was not blocked. Yet, the gH/gL binding kinetics were markedly different from that observed when pre-incubated with either orange community MAbs or no MAb (compare Fig. 9D to 9C). Whereas gH/gL binding normally exhibits a fast on- and off-rate (black curves) (21), its off-rate slowed considerably when it was pre-mixed with purple, red, or yellow MAbs (Fig. 9D,E). These results suggest that the red, purple, and yellow MAbs stabilize the gD-gH/gL binding complex.

The effects of anti-gH/gL MAbs on gD-gH/gL binding are dose-dependent.

Next, we tested if the effects of the anti-gH/gL MAbs on gD-gH/gL binding were dose-dependent. As in the previous figure, the level of gH/gL binding to gD in the absence of antibody is shown in each graph as a black curve. We used anti-gB MAb A22 (43), which does not bind to gD or gH/gL, as a control; as expected, it did not inhibit the binding of gH/gL to gD at any concentration tested (Fig. 10A).

In these studies, we found that MAb 53S inhibited gH/gL binding to gD in a dose-dependent manner, with binding partially reduced at the lowest concentration of IgG tested and binding was completely blocked by 0.2 mg/mL (Fig. 10B). MAb CHL17 blocked gD-gH/gL binding in a similar dose-dependent manner, with complete blocking by 0.4 mg/mL IgG (Fig. 10C). In contrast, blocking by MAb CHL18 was dose-dependent but not complete, even at the highest concentration tested (1mg/mL IgG) (Fig. 10D). One interpretation of these data is that the epitope of CHL18, which is at the C-terminus of gL (28), is only partially exposed (31) and therefore the MAb cannot fully access the epitope to prevent binding to gD.

MAb CHL2, which appeared to stabilize the gD-gH/gL interaction (Fig. 9E), did not block the interaction at any concentration tested (Fig. 10E). However, effects on the kinetics of gH/gL binding to gD were dose-dependent, with the off-rate appearing to be slower at higher concentrations of IgG (Fig. 10E). This effect was also observed with MAb CΔ48L3 (Fig. 10F).

Stabilization of the gD-gH/gL complex requires bivalent IgG.

The subset of anti-gH/gL MAbs that stabilized the gD-gH/gL complex were found in three communities (purple, red, yellow) whose epitopes are spread across the gH/gL molecule (Fig. 4), therefore this "function" cannot be localized to a single domain on the heterodimer. As each individual MAb (IgG) can bind to two antigens simultaneously, we asked whether the gD-gH/gL complex was stabilized through cross-linking of two gH/gL molecules. To address this question, we generated antigen-binding fragments (Fabs) that are capable of binding only one antigenic molecule. Hence, if cross-linking was a factor, pre-incubation of gH/gL with Fab would not stabilize gD-gH/gL complexes.

We generated Fabs for six of the anti-gH/gL MAbs tested in Fig. 9, representing five of the six MAb communities (CHL17, magenta; CHL27 and 53S, green; CΔ48L3, yellow; CHL2, red; CHL37, purple) (Fig. 2B). All Fabs were tested using SPR for gH/gL binding; unfortunately, the Fab generated from CHL18 (cyan community) did not bind to gH/gL and was omitted from this study (data not shown). We found that MAbs CHL2, CHL37, and CΔ48L3, which stabilized the complex as IgG, failed to do so as Fabs, there was no change in the off-rates of gH/gL/Fab on gD, and the binding curves overlapped that of gH/gL alone on gD (Fig. 11). For comparison, MAbs that blocked the gD-gH/gL interaction (CHL17, CHL27, 53S) did so as both Fabs (Fig. 11) and IgG (Fig. 9). We can draw two conclusions from this data. First, the ability

of MAbs to stabilize gH/gL binding to gD is due to the cross-linking of two separate gH molecules. Second, the ability of certain MAbs to block the gD-gH/gL interaction is not due to cross-linking, but more likely is due to interfering with the interaction itself. As such, we suggest that the epitopes of these MAbs overlap the gD binding site on gH/gL.

The effect of anti-gH/gL MAbs on cell-cell fusion.

Having characterized our panel of anti-gH2/gL2 MAbs, our goal was to use this information to determine the functional site on gH/gL that interacts with gD, thereby enabling gH/gL to be triggered to activate the fusion protein gB to drive fusion. To monitor fusion, we again used the SLA (Fig. 7E) (29, 40). Specifically, effector cells were transfected with gB2, gH2, gL2 and $Rluc8_{(1–7)}$ plasmids, while target cells expressing the gD receptor nectin-1 were transfected with $Rluc8_{(8–11)}$ plasmid. Effector cells were incubated with the luciferase substrate, incubated with the indicated IgG for 1 h before target cells were added, and fusion was triggered by the addition of soluble gD2(306t) and target cells. Luciferase activity was measured for 2 h and data were normalized to the 2h reading of the no antibody sample (Fig. 12A, black bar).

We found that orange community MAbs, which did not block gH/gL binding to gD, also did not block fusion (Fig. 12A), as was reported previously (28). With one exception (CΔ48L3), all MAbs that stabilized the gD-gH/gL interaction also inhibited fusion. To test whether the fusion inhibition was due to stabilization of gD-gH/gL complex, we also tested Fabs of these MAbs. The CHL2 Fab could neither stabilize the complex (Fig. 11) nor inhibit fusion (Fig. 12B). Surprisingly, although the CHL37 Fab did not stabilize the complex (Fig. 11), it still inhibited fusion (Fig. 12B), suggesting the existence of a third, as yet undetermined, mechanism of inhibiting gH/gL activity. All MAbs that blocked the interaction of gH/gL with gD inhibited

cell-cell fusion as both IgG and Fab (Fig. 12). Therefore, the blocking of gD-gH/gL complex formation has a functional consequence (the inhibition of fusion). Interestingly, Fabs 53S and CHL32 did not inhibit fusion as well as their IgG counterparts (Fig. 12), perhaps because the smaller Fabs were less able to sterically interfere with binding to gD.

The epitopes of anti-gH/gL MAbs that block gD binding identify a potential binding site for gD on gH/gL.

Having mapped the location of the epitopes of the anti-gH/gL MAbs that block the gD-gH/gL interaction, we used this information to identify the gD binding site on gH/gL (Fig. 13). Because the gH/gL crystal structure lacks the gH N-terminus and gL C-terminus, we used our modeled gH/gL structure that includes these regions (Fig. 2). When we examine the left side of gH/gL, the epitope MAb 53S (centered around gL residue 77) is in close proximity to those of MAbs CHL17/32 and CHL27 (Fig. 13A), all of which block the gD-gH/gL interaction. Turning the gH/gL molecule 180 degrees to the right side (Fig. 13B), the CHL18 epitope is now visible, along with more of the CHL17/32 and CHL27 epitopes. By looking at the gH/gL molecule from a "top-down" viewpoint, the epitopes of all five gD-gH/gL blocking MAbs are seen clustered together (Fig. 13C). We propose that this region, which contains portions of the gH N-terminus and much of gL, comprises the gD binding site on gH/gL.

Discussion

HSV entry and cell-cell fusion occur in a cascade of events involving the four essential glycoproteins: gD (the receptor binding protein), gH/gL (the key regulator of fusion), and gB

(the actual fusogen). Although it was theorized that gD transmitted the fusion triggering signal through direct interaction with gH/gL, the complex remained elusive (7, 20, 31, 44-47). In our previous study (21), we showed direct evidence that the gD ectodomain physically interacts with the ectodomain of gH/gL. The gD-gH/gL interaction was shown in real time using SPR and could be blocked by specific neutralizing and fusion-blocking anti-gD MAbs. By mapping the epitopes of these anti-gD MAbs that either allowed or blocked gD-gH/gL binding, we identified a potential gH/gL binding site on gD (Fig. 13D), located on the opposite face of the molecule as the receptor binding region.

In the present study, we turned our focus on gH/gL. gH/gL sits in the middle of the fusion cascade, interacting first with gD and subsequently with gB. gH/gL is the "bridge" between the receptor binding protein and the fusogen and has been proposed to regulate the fusion process (3, 7, 15, 31). To examine its physical interaction with gD, we used SPR and a panel of newly organized anti-gH/gL MAbs (28, 31, 33, 35, 48) in order to map those that blocked gD-gH/gL binding (Table 1). The epitopes of MAbs that blocked gH/gL binding to gD mapped to two presumably flexible regions, the N-terminus of gH and the C-terminus of gL. Because neither region was visible in the gH/gL crystal structure (9), we used 3D modeling to portray them (Fig. 2). The epitopes of CHL27 and CHL17/32 (gH N-terminus) and CHL18 (gL C-terminus), which block gD binding, created a continuous "patch" on this *in silico* model (Fig. 13C). These MAbs are in separate communities and do not compete for gH/gL binding, signifying that their epitopes are not overlapping (Fig. 2B). This group of epitopes neighbor that of another gD-blocking MAb, 53S, which is present on the "body" of gH/gL near gL residue 77 (Fig. 13C) and competes strongly with CHL27 (Fig. 2A, B). We conclude that the epitopes of these MAbs that block gD binding define the gD binding site on gH/gL, located at the N-

359 terminus of the heterodimer and involve both gH and gL residues. Our data are in agreement
360 with another study that suggested that the gD binding site on gH/gL was located within the N-
361 terminal half of gH (20). In that study, gH/gL chimeras containing segments of HSV-1 and
362 herpesvirus saimiri-1 proteins were tested for fusion and it was only when gD and the first two
363 domains of gH were from the same virus that the proteins were functional.

364 Four of the five anti-gH/gL MAbs that block binding to gD have epitopes that are located
365 on the flexible termini of gH (CHL17, CHL32, CHL27 on the N-terminus) or of gL (CHL18 on
366 the C-terminus) (Table 1). It had previously been postulated that these flexible regions may
367 move in response to gD binding, as a mutant form of gH missing the N-terminus (gHΔ48/gL)
368 was partially activated for fusion in a gD-independent fashion (31). Furthermore, MAbs with
369 epitopes on the C-terminus of gL that either did not inhibit or only weakly inhibited fusion
370 gained activity when the gH N-terminus was removed. These data lead to a model where the gH
371 N-terminus may partially occlude the gL C-terminus until the gH N-terminus is moved through
372 its binding to gD. Indeed, our *in silico* model of the complete gH/gL ectodomain places these
373 two regions next to each other (Fig. 13B). Movement of the gH N-terminus and the gL C-
374 terminus may be an important conformational step for the binding of gD and activation of
375 gH/gL.

376 We previously postulated that gH/gL has distinct "sides" for interacting with gD and gB,
377 although it is unknown if it can bind these molecules simultaneously. Current evidence suggests
378 that the gB binding region on gH/gL may be adjacent to the LP11 epitope (9), which is just
379 below the potential gD binding site (Fig. 7B). It is possible that gH/gL would need to disengage
380 from gD before binding gB. Unfortunately, the ectodomain of gB used in our experiments is in

the post-fusion form and there is no evidence that this form can bind to gH/gL (2, 21, 49, 50) unless both soluble proteins are treated with low pH and incubated with liposomes (51). Perhaps a membrane-bound, pre-fusion gB (52, 53) can be used to examine gH/gL-gB binding in future experiments.

Multiple MAbs in separate, non-competing antigenic communities stabilize the gD-gH/gL binding complex, as evidenced by their kinetics. When these IgGs were converted to Fabs, each MAb lost the ability to stabilize the observed gD-gH/gL complex. Stabilization may be explained by avidity, the notion that IgG (but not Fab) binding creates a bivalent gH/gL exhibiting a slower off rate because both molecules of gH/gL must disengage gD for the binding signal to disappear.

Numerous small-molecule inhibitors convey their physiological activity by stabilizing specific protein complexes (54). Stabilization of the gD-gH/gL complex does correlate with a functional MAb phenotype in some cases. When CHL2 is converted from IgG to Fab, it loses its ability to inhibit fusion (Fig. 12), suggesting that stabilization may be a mechanism of fusion inhibition. If the gD-gH/gL complex, which normally comes together and dissociates rapidly (21), is forced to stay together, this may affect the subsequent interaction of gH/gL with gB and break the fusion cascade. Interestingly, CHL37, which loses its ability to stabilize when converted to a Fab, is still able to inhibit cell-cell fusion (Fig. 12B). CHL37 may have a second mode of action beyond stabilization. MAbs against HSV glycoproteins that have multiple modes of action have been reported previously (e.g., anti-gD MAb MC23 blocks gD's interaction with both its receptor nectin-1 and gH/gL) (21, 55). Since CHL37 Fab does not stabilize or block the gD-gH/gL interaction, what is its mechanism of action for inhibiting cell-cell fusion? One hypothesis is that it could be preventing a conformational change in gH/gL needed to allow

interactions with gB. Since the epitope of CHL37 is located on the opposite side of gH/gL, distant from the proposed gH/gL-gB interaction domain (9), we do not believe that it is sterically blocking this interaction. Another possibility involves a caveat of our gD-gH/gL binding and cell-cell fusion assays. Whereas our binding assay uses the shorter form of gD, gD(285t), the longer gD(306t) is used in the fusion assay (see Materials and Methods). CHL37 may disrupt a function of the C-terminal gD(306t) tail.

We previously hypothesized that the gD binding region on gH/gL centered around the 52S epitope (gH amino acid 536) due to the inability of 52S to inhibit cell-cell fusion in a gD-independent system using a mutant gH (31, 33). Here, we show that MAbs CHL21 and CHL37, which compete with 52S, did not block gD-gH/gL binding. Yet, these MAbs both have an effect on gH/gL function and inhibit cell-cell fusion. If we assume that 52S, CHL21, and CHL37 have epitopes that are overlapping or in close proximity to each other and inhibit the same function of gH/gL, it would suggest that these MAbs impede an as-yet unknown function other than the binding of either gD or gB.

Clearly, structural information on the gD-gH/gL complex is required to define contact residues. Crystalization of the complex is not feasible due to the rapid off-rate of gH/gL on gD. One approach would be to use the stabilizing anti-gH/gL MAbs to “lock” the molecules together in order to visualize the complex. Although these MAbs lose their ability to stabilize the complex as Fabs, longer F(ab)2 fragments could be tested for this purpose. Once we enhance our understanding of the gD and gH/gL interface, this information will be useful to design targeted therapies that disrupt this interaction and inhibit the viral fusion cascade and HSV infection.

426

427 ## Materials and Methods

428 **Cells and soluble proteins.** All soluble proteins used in this study were purified from
429 baculovirus-infected insect (Sf9) cells. HSV type-2 gD(285t) and gD2(306t) were purified using
430 a DL6 immunosorbent column as described previously (22, 55, 56). The hexahistidine -tagged
431 proteins gH2/gL2 and gH1/gL1 (containing full-length gH ectodomains) and the N-terminal
432 truncation mutant gH2Δ48/gL2 were purified via nickel affinity chromatography (9, 51). B78-
433 H1 mouse melanoma cells were grown in Dulbecco modified Eagle medium (DMEM)
434 containing 5% fetal bovine serum (FBS) and 100 µg/ml of penicillin-streptomycin. For B78-
435 C10 cells (stably expressing nectin-1 receptor), medium was supplemented with 500 µg/ml of
436 Geneticin (G418) (57).

437

438 **Antibodies.** The following anti-gH/gL MAbs were used in this study: 46S, 52S, 53S (33, 35,
439 48); CHL2, CHL4-16, CHL17, CHL18, CHL29-31, CHL35, CHL37, CHL43 (28); LP11 (gift of
440 A. Minson) (33, 58); H6 (8); L4 (30); and CΔ48L3 (31). CHL21 and CHL27 were generated in
441 the same hybridoma fusion as the other CHL MAbs (28) but were previously uncharacterized.
442 To generate anti-gH/gL MAbs BBH2,3,4,5, mice were immunized with HSV-1 strain SC16.
443 Following fusion, hybridoma supernatants were screened by ELISA against soluble gH/gL
444 protein (59). Monoclonal antibody resistant (*mar*) mutants were generated using the
445 protocol described in Minson et al. (60). Anti-gD MAb 1D3 (55, 61, 62) was used to capture
446 soluble gD2(285t) to the biosensor chip. Anti-gB MAb A22 (43) was used as a negative control.
447 PAbs R137 and R176 were generated against purified gH1/gL1 and gH2/gL2, respectively (63,
448 64).

449

450 **Plasmid DNAs.** Plasmids pTC510 (gH2-WT), pTC579 (gL2-WT), pTC642 (gH2Δ48), pTC684
451 (gH2Δ64), pTC673 (gH2-R39A), pTC755 (gH2-T40A), pLF681 (gH2-Y41A), pTC712 (gH2-
452 R43A), pTC756 (gH2-D44A), and pCAGGS/MCS (a gift of P. G. Spear) were previously
453 described (34, 64-66). The remaining plasmids were generated by GenScript (Piscataway, NJ):
454 plasmids pTC1065 (gH2-WT) and pTC1066 (gL2-WT) were generated with optimized HSV-2
455 (333) codons and placed into vector pcDNA3.1 (EcoRI/HindIII); plasmids pDA1069 (gH2-
456 V161A), pDA1070 (gH2-T162A), pDA1071 (gL2-R46A), pDA1072 (gL2-D50A), pDA1073
457 (gL2-D51A), pDA1074 (gL2-P77A), pDA1075 (gL2-Q138A), pDA1076 (gL2-H142A), and
458 pDA1077 (gL2-P144A) were generated by site directed mutagenesis of pTC1065 (for gH2) or
459 pTC1066 (for gL2). Full-length plasmids used in the fusion assay [$Rluc8_{(1–7)}$, $Rluc8_{(8–11)}$, and
460 WT glycoprotein constructs pTC580 (gB2), pTC510 (gH2), pTC579 (gL2)] have all been
461 described previously (41, 64).

462

463 **Generating gH/gL MAb community maps using the continuous flow microspotter (CFM)/**
464 **surface plasmon resonance imaging (SPRi).** Epitope binning experiments of 36 anti-gH/gL
465 MAbs were performed on soluble gH2t/gL2 and gH1t/gL1 using the Carterra CFM/SPRi system.
466 We used a method described previously (24-26). Briefly, a CFM 2 was used to create a 48-spot
467 microarray of amine-coupled mAbs on a CDM200M sensor chip (Xantec GmbH). Upon docking
468 the printer chip into the SPR imager (IBIS MX96), the chip was blocked with ethanolamine and
469 the system primed with a running buffer of PBS-0.01% Tween 20. Epitope binning was
470 performed in a classical sandwich assay format using 100 nM soluble gH/gL as antigen, 100 nM
471 per MAb as analyte, and 1M glycine pH 2.0 for regeneration. All MAbs were tested in the role of

472 both analyte (in solution) and ligand (on chip). However, several MAbs were inactive as ligands
473 so their competitive profiles were determined solely from their performance as analytes. SPRi
474 data were processed in SPRint software and analyzed using Carterra's Epitope Binning 2.0
475 software for heat map generation, sorting, and network plotting. Binary sorting routines were
476 used to organize the heat maps and epitope bins were viewed as community network plots. All
477 experiments were performed at room temperature.

478

479 **Modeling of the full-length ectodomain of gH2/gL2.** The full length ectodomain structure of
480 HSV-2 gH was constructed using the Zhang lab's ITASSER web server (67) by inputting the
481 gH2 sequence (P89445) (68). The gH2/gL2 crystal structure (PDB ID: 3M1C) (9) was used as
482 the template to model the missing residues. gH2 residues 19-48,116-136 and 797-803 were now
483 visible in the 3D model. The same process was repeated to construct the full-length structure of
484 gL2 using the sequence (P28278) and the same structure (PDB ID: 3M1C) as the template to fill-
485 in the missing residues 17-23 and 166-224. The superimposed images of the model and crystal
486 structure of gH2, gL2, and the gH2/gL2 complex (Fig. S2 C, D, E) show that all missing loops
487 have been filled.

488

489 **CELISA.** To detect glycoprotein cell surface expression, we used a modified cell-based ELISA
490 (29, 40). B78 cells growing in clear 96-well plates (5×10^4 cells per well) were transfected
491 overnight with plasmids expressing gH2 and gL2. Cells were fixed with 3% paraformaldehyde
492 and rinsed with phosphate buffered saline (PBS) containing $Ca^{2+}$and Mg^{2+}**.** Cells were incubated
493 with the indicated primary antibodies diluted in 3% BSA-PBS and then incubated for 30 min

494 with goat anti-mouse secondary antibody coupled to horseradish peroxidase. Cells were rinsed
495 with 20 mM citrate buffer (pH 4.5), ABTS (2,2'-Azino-di(3-ethylbenzthiazoline) sulfonic acid
496 peroxidase substrate) substrate (Moss, Inc.) was added. The absorbance at 405 nm was recorded
497 using a BioTek plate reader.

498

499 **Split luciferase assay (SLA).** The SLA protocol has been described previously (29, 40, 69).
500 Briefly, 5×10^4 B78 cells (effector cells) were seeded on white, cell culture-treated 96-well
501 plates; 4×10^5 C10 cells (target cells) were seeded on 6-well plates. Transfection was performed
502 the following day. A master mix containing 125 ng each of the gB2, gH2, gL2, and $Rluc8_{(1-}$
503 $_{7)}$ plasmids was split over three wells of effector cells. Target cells were transfected with 1 µg of
504 $Rluc8_{(8-11)}$ plasmid/per well. Twenty-four hours post-transfection, effector cells were
505 preincubated for 1 h at 37°C with both EnduRen substrate (Promega) diluted 1:1,000 in fusion
506 medium (DMEM without phenol red supplemented with 50 mM HEPES and 5% FBS) and 20
507 µg/ml of MAb. Fusion was triggered by the addition of 50ug/ml soluble gD2(306t) and target
508 cells. Luciferase production was monitored over a 2 h period, with measurements taken every 5
509 min using a BioTek plate reader.

510

511 **Glycoprotein binding using the BIACORE 3000.** Experiments were carried out on a
512 BIACORE 3000 optical biosensor at 25°C following previous guidelines (55, 70, 71). All
513 injections were performed at a flow rate of 5 µL/min using HBS-EP buffer (10 mM HEPES, pH
514 7.4, 150 mM NaCl, 3 mM EDTA, 0.005% surfactant P20). After each experiment, the chip
515 surface was treated with brief pulses of 0.2 M Na_2CO_3 (pH 10) until the RU signal returned to

baseline (regeneration). First, the gH/gL binding-permissive anti-gD MAb 1D3 (IgG) (21) was amine-coupled to a CM5 sensor chip (GE Healthcare Bio-Sciences, Pittsburgh, PA). Second, 0.05 mg/mL of soluble, purified gD2(285t) was injected across the chip surface until approximately 150-300 RU was captured. Lastly, purified gH2t/gL2 (0.2 mg/ml) was injected for 240 s (analyte) and the binding was recorded. To test for blocking of gD-gH/gL binding via anti-gH/gL MAbs, soluble gH2/gL2 was pre-incubated with 0.6 mg/mL IgG or Fab at RT for 10 min before flowing the mixture across the captured gD2(285t).

Western blotting. B78-C10 cells were transfected with the desired plasmids according to the GenePORTER protocol (Gene Therapy Systems, Inc.). At 24 h post-transfection, cells were lysed in 10 mM Tris (pH 8)-150 mM NaCl-10 mM EDTA-1% NP-40-0.5% deoxycholic acid-1 mM phenylmethylsulfonyl fluoride. Typically, 5% of the total cell extract (from a single well of a 6-well plate) was separated by electrophoresis on a sodium dodecyl sulfate (SDS)-12% polyacrylamide gel. Proteins were detected by Western blotting onto nitrocellulose and probing with the desired counter-antibody.

Peptide ELISA. Synthetic 20-mer peptides were purchased from Mimotopes Pty. Ltd. (Melbourne, Australia) and described previously (28). Fifty microliters of an approximately 1 μM concentration (in PBS) of each peptide was placed in each well of a 96-well Reacti-bind high-binding-capacity streptavidin-coated plate (Pierce) and incubated for 1 h. The plate was then blocked with 200 μl of 5% milk-PBS-T for 30 min and probed with 50 μl of 20 μg/ml MAb

for 1 h in milk-PBS-T. All steps were performed at room temperature. Bound IgG was visualized with goat anti-mouse IgG-horseradish peroxidase.

Acknowledgements

The authors dedicate this article to the memory of our friend Roselyn J. Eisenberg. Roz was a world-class scientist, known for her groundbreaking HSV research in the lab she co-ran for decades with Gary H. Cohen. She was integral to the development of this manuscript and will be sorely missed by all of her friends, students, and mentees. Her contribution to this paper was testimony to her love of research.

We thank Leslie King, Beth Schachter, and Jeannie Hirsch for critical readings of the manuscript.

This research was supported by AI-18289, AI-142940, AI-139618, and a grant from BIONTECH, Inc. (to G.H.C.) and NSF grants RUI-1904797/ACI-1429467 and XSEDE MCB 170088 (to C.W.) and The Wellcome Trust, UK (to H. B.).

N.T.D. is employed by Carterra, Inc.

B.D.B. is employed by Inovan, Inc.

555 **Table 1:** Properties of αgH/gL MAbs

MAb	Community/ Sub-community	Type	Epitope Residues	Competes with	Blocks gD-gH/gL binding	Stabilizes gD-gH/gL	Blocks fusion (SLA)
CHL27	green	TC	gH 37-47	53S	Yes	No	Yes
53S	green	TC	gL 48[a], 55[a], 77	CHL27, LP11, BBH3	Yes	No	Yes
CHL17	magenta	T2S	gH 19-38[b]	CHL32	Yes	No	Yes
CHL32	magenta	T2S	gH 19-38[b]	CHL17	Yes	No	Yes
CHL21	purple	TC	ND[c]	CHL37, 52S, 46S, BBH5	No	Yes	Yes
CHL37	purple	TC	ND	CHL21, 52S, 46S, BBH5	No	Yes	Yes
CHL29	orange	TC	gH 676-686[b]	CHL30	No	No	No
CHL35	orange	TC	gH 145-155[b]	CHL31	No	No	No
CHL2	red	T2S	gH 116[b]	CHL4-16	No	Yes	Yes
CΔ48L3	yellow	T2S	gL 173-183[d]	-	No	Yes	No[e]
CHL18	cyan	T2S	gL 209-218[b]	-	Yes (50%)	No	Yes (50%)

556 [a] Fan et al. (39)

557 [b] Cairns et al. (28)

558 [c] ND, not determined

559 [d] Atanasiu et al. (31)

560 [e] blocks gD-constitutive fusion for gH2Δ48 & gH2Δ29 >50% but not WT-gH2 (31)

561

Figure Legends

Fig 1. Binning of anti-gH/gL MAbs. (A) Graphical representation of the Carterra Continuous Flow Microspotter (CFM)/SPRi protocol. The individual anti-gH/gL MAbs are printed to distinct spots on the biosensor chip (shown as distinctly colored Ys). The antigen (gH/gL, orange/blue ovals) is then flowed across the chip surface and captured by each MAb. Next, the first anti-gH/gL MAb (analyte) is flowed across the chip surface and its binding capacity measured. Then, the chip surface is regenerated back down to the level of the printed MAbs and the cycle is repeated for each individual MAb to be tested. (B, D) Heat maps. Red boxes denote competition between the ligand MAb and the analyte MAb. Black boxes indicate self-self MAb competition. Green boxes indicate no competition between MAbs and a high level of binding of the analyte MAb onto gH/gL as bound by the ligand MAb. Yellow boxes show a lower level of binding for the analyte, but the MAbs are still scored as not competing. Excluded from analysis: ligand MAbs that bound ≤10 response units of gH/gL (grey boxes); MAbs that blocked all other MAbs. Values in each box designate the difference in the normalized y-scale values of the MAb injections compared to the antigen/buffer injections; the value is taken at the x-scale position where the measurement bar is placed. x-axis, ligands; y-axis, analytes. MAb names are colored according to community groupings as shown in the combined dendrograms (C, E). Horizontal lines at the base of the denogram indicate distinct bins of MAbs, i.e. they have identical competition profiles. MAb communities (denoted with colored rectangles) were chosen based on the dendogram cut-off (dotted horizontal line); cut-off was chosen so as to give five different communities on each type of gH/gL (black dots).

584 **Fig. 2**: **Antigenic community maps for HSV gH1/gL1 and gH2/gL2.** For HSV-1 gH/gL (A)
585 and HSV-2 gH/gL (B), the MAbs were divided into four communities based on dendogram
586 estimations (Fig. 1C, 1E) and colored accordingly. Antibody names in a circle indicate that
587 competition was measured as both a ligand and an analyte; antibody names in a square indicate
588 that competition was measured in one direction only, as either a ligand or an analyte. Solid
589 connecting lines specify that competition between the two MAbs was seen as both a ligand and
590 analyte for each, while dashed connecting lines indicate competition in one direction only. The
591 purple community for gH2/gL2 was further divided into magenta, orange, and purple sub-
592 communities according to previous data (28). Asterisks (*) highlight MAbs that are "type-
593 common" and bind to both gH1/gL1 and gH2/gL2.

594

595 **Fig. 3. gH2/gL2 3D model comparison with gH2/gL2 crystal structure.** (A) The gH2
596 ectodomain protein sequence view. Amino acid numbers are displayed along the top. The signal
597 peptide (residues 1-18) was removed for model determination. The sequence on top represents
598 the fully constructed gH2 model while the sequence underneath represents the crystal structure
599 with missing residues represented as "~" (19-48, 116-136, and 798-803). Beta sheets are
600 depicted with a blue arrow, and alpha-helices with a red cylinder. A similar view is shown for
601 gL2 (B), where residues 1-16 encompass the signal peptide and the missing crystal structure
602 residues span 17-23 and 166-224. (C) Superimposition of the gH2/gL2 crystal structure (PDB:
603 3M1C) (green) and the fully constructed ectodomain model (red). The image on the left shows
604 only the portions of the model that overlap with the crystal structure. The image on the right
605 displays the fully constructed model with the missing residues shown in blue. (D) Surface view

606 of the gH2/gL2 complex, with gH shown in white, gL in gray, and missing gH/gL residues
607 shown in blue.

608

609 **Fig. 4**: **Positioning of MAb epitope communities onto a 3D structural model of the full-**
610 **length gH2/gL2 ectodomain.** Surface representation of gH2 is shown in white while gL2 is
611 shown in grey. The structure is rotated 180^{o} between (A) and (B). Antibody-resistant mutations
612 for individual MAbs and peptide mapping data (28, 31, 33) were used to position the colored
613 MAb communities (red, magenta, orange, cyan, yellow and purple) from Fig. 1C onto the
614 structural model. These residues are similarly colored on the surface of the gH2/gL2 structure to
615 convey points of orientation. Due to the large number of MAbs within the red community, only
616 CHL2 is shown. MAbs CHL21 and CHL37, which strongly compete with type-1 MAbs 52S and
617 BBH5, are positioned above the MAb-resistant mutations for 52S (gH 536) (33) and BBH5 (gH
618 732), shown on the structure in purple. MAbs CHL27 was mapped to gH residues 37-47 and
619 MAb 53S to gL residue 77 as shown in subsequent figures.

620

621 **Fig 5. Epitope mapping: characterization of MAbs CHL21 and CHL37.** (A) Western blot
622 analysis. Soluble gH/gL proteins were run under either native (N) or denaturing (D) conditions.
623 Blots were probed with the indicated antibodies. R137 was used as the PAb against gH1/gL1,
624 and R176 as the PAb against gH2/gL2 and gH2Δ48/gL2. Molecular weight markers are
625 designated with lines and shown to the left in kDa. (B) SPR analysis of gH/gL binding. Anti-
626 HIS IgG was coupled to a biosensor chip. Next, soluble, purified gH1/gL1 (grey), gH2/gL2
627 (black), or gH2Δ48/gL2 (brown) was captured via C-terminal 6-HIS tags. Curves show binding

628 of the indicated MAb to the immobilized proteins. Each experiment was done at least twice,
629 representative experiment shown.

630

631 **Fig 6. Epitope mapping: characterization of MAb CHL27.** (A) SPR analysis of MAb
632 binding to gH/gL. Procotol is as outlined in Fig. 5B. (B) Peptide ELISA using MAb CHL27.
633 gH2 peptides were biotinylated at the N-terminus, which facilitated binding to a 96-well
634 streptavidin-coated plate. Each well was probed with CHL27 and visualized with goat anti-
635 mouse IgG-horseradish peroxidase. (C) N-terminal amino acid sequence of gH2, with amino
636 acid numbers shown below. The signal sequence (residues 1-18) and the CHL27 binding region
637 (residues 37-47) are indicated with underlines. The sequence deleted in the gH2Δ48 construct is
638 indicated with a bracket above the sequence. gH residues highlighted in green are important for
639 CHL27 binding, as shown by Western blot (D). Cells were transfected with the desired plasmids
640 and cell lysates were separated by electrophoresis via SDS-PAGE. Lysates from cells transfected
641 with empty plasmid (vector) and gL only served as negative controls. Antibodies used during
642 Western blotting are shown to the right of each blot (anti-gH/gL PAb R176 and MAb CHL27).

643

644 **Fig. 7**: **Characterization of gH and gL mutants used to identify the 53S epitope.** (A)
645 Competition tree. Arrows indicate competition for binding to gH/gL, while no arrows between
646 MAbs signify no competition. Data from SPR analysis (Carterra, Fig. 1 and BIACORE 3000,
647 data not shown) was used to make the tree. MAbs are colored according to their community
648 groups in Fig. 2. (B) Selection of gH2 and gL2 point mutations to test for 53S reactivity.
649 Residues are mapped onto our 3D model of the gH2/gL2 ectodomain (Fig. 3). Amino acids

indicated in green were mutated to alanine. The locations of monoclonal antibody resistant mutations for MAbs CHL27 (gH residues 39, 41, 43, 44; olive), LP11 (gH1 residues 168, 329; blue), BBH2/4 (gH1 residue 175; blue) and BBH3 (gH1 residues 370, 371; orange) are also shown. gH2 is shown in white and gL2 in grey. (C) Cells transfected with WT or mutant gH2 or gL2 constructs were analyzed by Western blotting under denaturing conditions of SDS-PAGE, using the anti-gHgL PAb R176. Total extracts from cells transfected with empty plasmid (vector) served as a negative control. Position of gH and gL on the blot is indicated on the right. (D) Cell-surface ELISA (CELISA). C10 cells were transfected with WT or mutant constructs and tested for their reactivity to MAb 53S. Total levels of expression were determined with MAbs CΔ48L3 (anti-gL) and CHL27 (anti-gH). (E) Cell-cell fusion activity as measured by split luciferase assay (SLA). B78 effector cells were transfected with gB2, gH2, gL2, and $Rluc8_{(1–7)}$ plasmids, while C10 target cells were transfected with $Rluc8_{(8–11)}$ plasmid. 24 h post-transfection, effector cells were incubated with substrate for 1 h. Target cells were then transferred to effector cells, with soluble gD2(306t) added at the same time to trigger fusion. Luciferase production was measured for 2 h. For CELISA and SLA, all mutants were tested in duplicate. Error bars represent standard error. Mutant gL-P77A, a potential 53S *mar*, is highlighted in (C-E) in green.

Fig. 8: **Demonstration of gH2/gL2 binding to gD2, as detected by SPR.** (A) Schematic diagram of the SPR protocol. Anti-gD MAb 1D3, which is permissive for gH/gL binding (21), was coupled to a CM5 biosensor chip. Sequential injections of soluble gD2(285t) and soluble gH2/gL2 were performed. An increase in resonance units (RU) after the gH/gL injection indicated gH/gL binding (red box) (B). The RU from a control flow cell where only gH/gL was injected (no gD) was subtracted.

673

674 **Fig. 9**: **Effect of anti-gH/gL MAbs on gD-gH/gL binding.** (A) Schematic diagram of the SPR
675 protocol. Anti-gD MAb 1D3 was coupled to a CM5 biosensor chip and then soluble gD2(285t)
676 was injected across the flow cell. Next, either gH2/gL2 alone or gH2/gL2 that was preincubated
677 with 0.4 mg/mL of the indicated MAb (IgG) was injected cross the flow cell. The RU from a
678 control flow cell where only gH/gL or gH/gL + IgG was injected (no gD) was subtracted from
679 each. (B) MAbs that block gH/gL binding to gD. (C) MAbs that do not affect gD-gH/gL
680 binding. (D) MAbs that stabilize the gD-gH/gL binding. Only the gH/gL binding portion of the
681 curves (Fig. 8B, red box) are shown in parts (B-E). Black curves show gH/gL binding to gD
682 when no MAb is added (positive control). Curves where gH/gL was pre-incubated with MAbs
683 are colored according to their MAb community in Fig. 2B. Each experiment was done at least
684 twice, representative experiment shown.

685

686 **Fig. 10. Blocking of gH2/gL2 binding by anti-gH/gL MAbs is dose-responsive.** The SPR
687 protocol was as outlined in Fig 9A. Soluble gH2/gL2 was preincubated with a range of IgG
688 concentrations as listed to the right of each set of curves: (A) Control IgG (anti-gB MAb A22);
689 (B) 53S; (C) CHL17; (D) CHL18; (E) CHL2; (F) CD48L3. The RU from a control flow cell
690 where only gH/gL or gH/gL + IgG was injected (no gD) was subtracted from each. Only the
691 gH/gL binding portion of the curves are shown. Black curves show gH/gL binding to gD when
692 no MAb is added (positive control). Colored curves represent the same IgG concentration as
693 shown in Fig. 9 (0.4 mg/mL).

694

695 **Fig. 11. Effect of anti-gH/gL Fabs on gH2/gL2 binding to gD2.** Experiments were set up as
696 outlined in Fig. 9A. Anti-gD MAb 1D3 was coupled to a CM5 biosensor chip and then soluble
697 gD2(285t) was injected across the flow cell. Next, either gH2/gL2 alone or gH2/gL2 that was
698 preincubated with 0.6 mg/mL of the indicated Fab was injected cross the flow cell. Fab
699 concentration was chosen so it was in excess. The RU from a control flow cell where only
700 gH/gL or gH/gL + Fab was injected (no gD) was subtracted from each. Only gH/gL binding
701 curves are shown. Black curves show gH/gL binding to gD when no Fab is added (positive
702 control). Curves where gH/gL was pre-incubated with Fabs are colored according to their MAb
703 community in Fig. 2B.

704

705 **Fig. 12. Effect of anti-gH/gL MAbs on cell-cell fusion as measured by the split luciferase**
706 **assay (SLA).** B78 effector cells were transfected with gB2, gH2, gL2, and $Rluc8_{(1–7)}$ plasmids,
707 while C10 target cells were transfected with $Rluc8_{(8–11)}$ plasmid. 24 h post-transfection, effector
708 cells were incubated with substrate and either IgG (A) or Fab (B) for 1 h. Target cells were then
709 transferred to effector cells, with soluble gD2(306t) added to trigger fusion. Luciferase
710 production was measured for 2 h. All antibodies were tested a minimum of two times. Error bars
711 represent standard error. Anti-myc MAb was used as a negative control (gray bar). MAbs are
712 colored according to their community as shown in Fig. 2B.

713

714 **Fig. 13. Localization of the gD binding site on a gH/gL 3D modeled structure.** The gH/gL
715 model is rotated 180^{o} between (A) and (B). gH is shown in white and gL in grey. Residues
716 within each of the following MAb epitopes are highlighted by color: CHL17/32 (gH residues 19-

38; magenta); CHL27 (gH residues 39, 41, 43, 44; olive); 53S (gL residue 77; green); and CHL18 (gL residues 209-219; cyan). To orient the molecule, the gH N- and C-termini are highlighted in yellow. In (C), gH/gL is uniformly colored white and positioned from the "top" so as the epitopes that define the gD binding region (black dotted circle) can be viewed together. The gL N-and C-termini are highlighted in yellow, along with the gH N-terminus. (D) Surface representation of the gD crystal structure (PDB: 2C36). Antibody-resistant mutations that were used to position the epitopes of anti-gD MAbs that block gH/gL binding are colored on the structure (MC5, blue; MC23, red; MC14, brown) (21). The gH/gL binding region is marked with a dashed circle.

References

1. Atanasiu D, Saw WT, Cohen GH, Eisenberg RJ. 2010. Cascade of events governing cell-cell fusion induced by herpes simplex virus glycoproteins gD, gH/gL, and gB. J Virol 84:12292-12299.
2. Heldwein EE, Krummenacher C. 2008. Entry of herpesviruses into mammalian cells. Cell Mol Life Sci 65:1653-68.
3. Vollmer B, Grunewald K. 2020. Herpesvirus membrane fusion - a team effort. Curr Opin Struct Biol 62:112-120.
4. Eisenberg RJ, Atanasiu D, Cairns TM, Gallagher JR, Krummenacher C, Cohen GH. 2012. Herpes virus fusion and entry: a story with many characters. Viruses 4:800-32.
5. Krummenacher C, Carfi A, Eisenberg RJ, Cohen GH. 2013. Entry of herpesviruses into cells: the enigma variations. Adv Exp Med Biol 790:178-95.
6. Connolly SA, Jackson JO, Jardetzky TS, Longnecker R. 2011. Fusing structure and function: a structural view of the herpesvirus entry machinery. Nat Rev Microbiol 9:369-81.
7. Vallbracht M, Backovic M, Klupp BG, Rey FA, Mettenleiter TC. 2019. Common characteristics and unique features: A comparison of the fusion machinery of the alphaherpesviruses Pseudorabies virus and Herpes simplex virus. Adv Virus Res 104:225-281.
8. Peng T, Ponce de Leon M, Novotny MJ, Jiang H, Lambris JD, Dubin G, Spear PG, Cohen GH, Eisenberg RJ. 1998. Structural and antigenic analysis of a truncated form of the herpes simplex virus glycoprotein gH-gL complex. J Virol 72:6092-103.
9. Chowdary TK, Cairns TM, Atanasiu D, Cohen GH, Eisenberg RJ, Heldwein EE. 2010. Crystal structure of the conserved herpesvirus fusion regulator complex gH-gL. Nat Struct Mol Biol 17:882-888.

10. Roop C, Hutchinson L, Johnson DC. 1993. A mutant herpes simplex virus type 1 unable to express glycoprotein L cannot enter cells, and its particles lack glycoprotein H. J Virol 67:2285-97.
11. Hutchinson L, Browne H, Wargent V, Davis-Poynter N, Primorac S, Goldsmith K, Minson AC, Johnson DC. 1992. A novel herpes simplex virus glycoprotein, gL, forms a complex with glycoprotein H (gH) and affects normal folding and surface expression of gH. J Virol 66:2240-50.
12. Atanasiu D, Whitbeck JC, de Leon MP, Lou H, Hannah BP, Cohen GH, Eisenberg RJ. 2010. Bimolecular complementation defines functional regions of herpes simplex virus gB that are involved with gH/gL as a necessary step leading to cell fusion. J Virol 84:3825-3834.
13. Stampfer SD, Heldwein EE. 2013. Stuck in the middle: structural insights into the role of the gH/gL heterodimer in herpesvirus entry. Curr Opin Virol 3:13-9.
14. Heldwein EE. 2016. gH/gL supercomplexes at early stages of herpesvirus entry. Curr Opin Virol 18:1-8.
15. Atanasiu D, Saw WT, Eisenberg RJ, Cohen GH. 2016. Regulation of herpes simplex virus glycoprotein-induced cascade of events governing cell-cell fusion. J Virol 91:10535-10544.
16. Carfi A, Willis SH, Whitbeck JC, Krummenacher C, Cohen GH, Eisenberg RJ, Wiley DC. 2001. Herpes simplex virus glycoprotein D bound to the human receptor HveA. Mol Cell 8:169-79.
17. Di Giovine P, Settembre EC, Bhargava AK, Luftig MA, Lou H, Cohen GH, Eisenberg RJ, Krummenacher C, Carfi A. 2011. Structure of herpes simplex virus glycoprotein D bound to the human receptor nectin-1. PLoS Pathog 7:e1002277.
18. Lu G, Zhang N, Qi J, Li Y, Chen Z, Zheng C, Gao GF, Yan J. 2014. Crystal structure of herpes simplex virus 2 gD bound to nectin-1 reveals a conserved mode of receptor recognition. J Virol 88:13678-88.
19. Krummenacher C, Supekar VM, Whitbeck JC, Lazear E, Connolly SA, Eisenberg RJ, Cohen GH, Wiley DC, Carfi A. 2005. Structure of unliganded HSV gD reveals a mechanism for receptor-mediated activation of virus entry. Embo J 24:4144-53.
20. Fan Q, Longnecker R, Connolly SA. 2015. A Functional Interaction between Herpes Simplex Virus 1 Glycoprotein gH/gL Domains I and II and gD Is Defined by Using Alphaherpesvirus gH and gL Chimeras. J Virol 89:7159-69.
21. Cairns TM, Ditto NT, Atanasiu D, Lou H, Brooks BD, Saw WT, Eisenberg RJ, Cohen GH. 2019. Surface Plasmon Resonance Reveals Direct Binding of Herpes Simplex Virus Glycoproteins gH/gL to gD and Locates a gH/gL Binding Site on gD. J Virol 93.
22. Rux AH, Willis SH, Nicola AV, Hou W, Peng C, Lou H, Cohen GH, Eisenberg RJ. 1998. Functional region IV of glycoprotein D from herpes simplex virus modulates glycoprotein binding to the herpesvirus entry mediator. J Virol 72:7091-8.
23. Gallagher JR, Saw WT, Atanasiu D, Lou H, Eisenberg RJ, Cohen GH. 2013. Displacement of the C-terminus of herpes simplex virus gD is sufficient to expose the fusion activating interfaces on gD. J Virol doi:10.1128/JVI.01727-13.
24. Cairns TM, Ditto NT, Lou H, Brooks BD, Atanasiu D, Eisenberg RJ, Cohen GH. 2017. Global sensing of the antigenic structure of herpes simplex virus gD using high-throughput array-based SPR imaging. PLoS Pathog 13:e1006430.
25. Abdiche YN, Harriman R, Deng X, Yeung YA, Miles A, Morishige W, Boustany L, Zhu L, Izquierdo SM, Harriman W. 2016. Assessing kinetic and epitopic diversity across orthogonal monoclonal antibody generation platforms. MAbs 8:264-77.
26. Abdiche YN, Miles A, Eckman J, Foletti D, Van Blarcom TJ, Yeung YA, Pons J, Rajpal A. 2014. High-throughput epitope binning assays on label-free array-based biosensors can yield exquisite epitope discrimination that facilitates the selection of monoclonal antibodies with functional activity. PLoS One 9:e92451.

27. Brooks BD, Miles AR, Abdiche YN. 2014. High-throughput epitope binning of therapeutic monoclonal antibodies: why you need to bin the fridge. Drug Discov Today 19:1040-4.
28. Cairns TM, Shaner MS, Zuo Y, Ponce-de-Leon M, Baribaud I, Eisenberg RJ, Cohen GH, Whitbeck JC. 2006. Epitope mapping of herpes simplex virus type 2 gH/gL defines distinct antigenic sites, including some associated with biological function. J Virol 80:2596-608.
29. Atanasiu D, Saw WT, Gallagher JR, Hannah BP, Matsuda Z, Whitbeck JC, Cohen GH, Eisenberg RJ. 2013. Dual split protein-based fusion assay reveals that mutations to herpes simplex virus (HSV) glycoprotein gB alter the kinetics of cell-cell fusion induced by HSV entry glycoproteins. J Virol 87:11332-45.
30. Dubin G, Jiang H. 1995. Expression of herpes simplex virus type 1 glycoprotein L (gL) in transfected mammalian cells: evidence that gL is not independently anchored to cell membranes. J Virol 69:4564-8.
31. Atanasiu D, Cairns TM, Whitbeck JC, Saw WT, Rao S, Eisenberg RJ, Cohen GH. 2013. Regulation of herpes simplex virus gB-induced cell-cell fusion by mutant forms of gH/gL in the absence of gD and cellular receptors. MBio 4.
32. Cohen GH, Isola VJ, Kuhns J, Berman PW, Eisenberg RJ. 1986. Localization of discontinuous epitopes of herpes simplex virus glycoprotein D: use of a nondenaturing ("native" gel) system of polyacrylamide gel electrophoresis coupled with Western blotting. J Virol 60:157-66.
33. Gompels UA, Carss AL, Saxby C, Hancock DC, Forrester A, Minson AC. 1991. Characterization and sequence analyses of antibody-selected antigenic variants of herpes simplex virus show a conformationally complex epitope on glycoprotein H. J Virol 65:2393-401.
34. Cairns TM, Friedman LS, Lou H, Whitbeck JC, Shaner MS, Cohen GH, Eisenberg RJ. 2007. N-terminal mutants of herpes simplex virus type 2 gH are transported without gL but require gL for function. J Virol 81:5102-11.
35. Showalter SD, Zweig M, Hampar B. 1981. Monoclonal antibodies to herpes simplex virus type 1 proteins, including the immediate-early protein ICP 4. Infect Immun 34:684-92.
36. Fuller AO, Santos RE, Spear PG. 1989. Neutralizing antibodies specific for glycoprotein H of herpes simplex virus permit viral attachment to cells but prevent penetration. J Virol 63:3435-43.
37. Cairns TM, Milne RS, Ponce-de-Leon M, Tobin DK, Cohen GH, Eisenberg RJ. 2003. Structure-function analysis of herpes simplex virus type 1 gD and gH-gL: clues from gDgH chimeras. J Virol 77:6731-42.
38. Klyachkin YM, Stoops KD, Geraghty RJ. 2006. Herpes simplex virus type 1 glycoprotein L mutants that fail to promote trafficking of glycoprotein H and fail to function in fusion can induce binding of glycoprotein L-dependent anti-glycoprotein H antibodies. J Gen Virol 87:759-67.
39. Fan Q, Lin E, Spear PG. 2009. Insertional mutations in herpes simplex virus type 1 gL identify functional domains for association with gH and for membrane fusion. J Virol 83:11607-15.
40. Saw WT, Matsuda Z, Eisenberg RJ, Cohen GH, Atanasiu D. 2015. Using a split luciferase assay (SLA) to measure the kinetics of cell-cell fusion mediated by herpes simplex virus glycoproteins. Methods 90:68-75.
41. Ishikawa H, Meng F, Kondo N, Iwamoto A, Matsuda Z. 2012. Generation of a dual-functional split-reporter protein for monitoring membrane fusion using self-associating split GFP. Protein Eng Des Sel 25:813-20.
42. Atanasiu D, Saw WT, Lazear E, Whitbeck JC, Cairns TM, Lou H, Eisenberg RJ, Cohen GH. 2018. Using antibodies and mutants to localize the presumptive gH/gL binding site on HSV gD. J Virol doi:10.1128/JVI.01694-18.

43. Bender FC, Samanta M, Heldwein EE, de Leon MP, Bilman E, Lou H, Whitbeck JC, Eisenberg RJ, Cohen GH. 2007. Antigenic and mutational analyses of herpes simplex virus glycoprotein B reveal four functional regions. J Virol 81:3827-41.
44. Fan Q, Longnecker R, Connolly SA. 2014. Substitution of herpes simplex virus 1 entry glycoproteins with those of saimiriine herpesvirus 1 reveals a gD-gH/gL functional interaction and a region within the gD profusion domain that is critical for fusion. J Virol 88:6470-82.
45. Atanasiu D, Whitbeck JC, Cairns TM, Reilly B, Cohen GH, Eisenberg RJ. 2007. Bimolecular complementation reveals that glycoproteins gB and gH/gL of herpes simplex virus interact with each other during cell fusion. Proc Natl Acad Sci U S A 104:18718-23.
46. Gianni T, Amasio M, Campadelli-Fiume G. 2009. Herpes simplex virus gD forms distinct complexes with fusion executors gB and gH/gL through the C-terminal profusion. J Biol Chem.
47. Perez-Romero P, Perez A, Capul A, Montgomery R, Fuller AO. 2005. Herpes simplex virus entry mediator associates in infected cells in a complex with viral proteins gD and at least gH. J Virol 79:4540-4.
48. Gompels UA, Minson AC. 1989. Antigenic properties and cellular localization of herpes simplex virus glycoprotein H synthesized in a mammalian cell expression system. J Virol 63:4744-55.
49. Heldwein EE, Lou H, Bender FC, Cohen GH, Eisenberg RJ, Harrison SC. 2006. Crystal structure of glycoprotein B from herpes simplex virus 1. Science 313:217-20.
50. Backovic M, Jardetzky TS. 2009. Class III viral membrane fusion proteins. Curr Opin Struct Biol 19:189-196.
51. Cairns TM, Whitbeck JC, Lou H, Heldwein EE, Chowdary TK, Eisenberg RJ, Cohen GH. 2011. Capturing the herpes simplex virus core fusion complex (gB-gH/gL) in an acidic environment. J Virol 85:6175-84.
52. Fontana J, Atanasiu D, Saw WT, Gallagher JR, Cox RG, Whitbeck JC, Brown LM, Eisenberg RJ, Cohen GH. 2017. The Fusion Loops of the Initial Prefusion Conformation of Herpes Simplex Virus 1 Fusion Protein Point Toward the Membrane. mBio 8.
53. Zeev-Ben-Mordehai T, Vasishtan D, Hernandez Duran A, Vollmer B, White P, Prasad Pandurangan A, Siebert CA, Topf M, Grunewald K. 2016. Two distinct trimeric conformations of natively membrane-anchored full-length herpes simplex virus 1 glycoprotein B. Proc Natl Acad Sci U S A 113:4176-81.
54. Andrei SA, Sijbesma E, Hann M, Davis J, O'Mahony G, Perry MWD, Karawajczyk A, Eickhoff J, Brunsveld L, Doveston RG, Milroy LG, Ottmann C. 2017. Stabilization of protein-protein interactions in drug discovery. Expert Opin Drug Discov 12:925-940.
55. Lazear E, Whitbeck JC, Ponce-de-Leon M, Cairns TM, Willis SH, Zuo Y, Krummenacher C, Cohen GH, Eisenberg RJ. 2012. Antibody-induced conformational changes in herpes simplex virus glycoprotein gD reveal new targets for virus neutralization. J Virol 86:1563-76.
56. Nicola AV, Willis SH, Naidoo NN, Eisenberg RJ, Cohen GH. 1996. Structure-function analysis of soluble forms of herpes simplex virus glycoprotein D. J Virol 70:3815-22.
57. Milne RS, Connolly SA, Krummenacher C, Eisenberg RJ, Cohen GH. 2001. Porcine HveC, a member of the highly conserved HveC/nectin 1 family, is a functional alphaherpesvirus receptor. Virology 281:315-328.
58. Buckmaster EA, Gompels U, Minson A. 1984. Characterisation and physical mapping of an HSV-1 glycoprotein of approximately 115 X 10(3) molecular weight. Virology 139:408-13.
59. Parry C, Bell S, Minson T, Browne H. 2005. Herpes simplex virus type 1 glycoprotein H binds to alphavbeta3 integrins. J Gen Virol 86:7-10.
60. Minson AC, Hodgman TC, Digard P, Hancock DC, Bell SE, Buckmaster EA. 1986. An analysis of the biological properties of monoclonal antibodies against glycoprotein D of herpes simplex virus

and identification of amino acid substitutions that confer resistance to neutralization. J Gen Virol 67:1001-1013.

61. Eisenberg RJ, Long D, Pereira L, Hampar B, Zweig M, Cohen GH. 1982. Effect of monoclonal antibodies on limited proteolysis of native glycoprotein gD of herpes simplex virus type 1. J Virol 41:478-488.

62. Friedman HM, Cohen GH, Eisenberg RJ, Seidel CA, Cines DB. 1984. Glycoprotein C of herpes simplex virus 1 acts as a receptor for the C3b complement component on infected cells. Nature 309:633-5.

63. Peng T, Ponce-de-Leon M, Jiang H, Dubin G, Lubinski JM, Eisenberg RJ, Cohen GH. 1998. The gH-gL complex of herpes simplex virus (HSV) stimulates neutralizing antibody and protects mice against HSV type 1 challenge. J Virol 72:65-72.

64. Cairns TM, Landsburg DJ, Whitbeck JC, Eisenberg RJ, Cohen GH. 2005. Contribution of cysteine residues to the structure and function of herpes simplex virus gH/gL. Virology 332:550-62.

65. Okuma K, Nakamura M, Nakano S, Niho Y, Matsuura Y. 1999. Host range of human T-cell leukemia virus type I analyzed by a cell fusion-dependent reporter gene activation assay. Virology 254:235-244.

66. Pertel PE, Fridberg A, Parish ML, Spear PG. 2001. Cell fusion induced by herpes simplex virus glycoproteins gB, gD, and gH-gL requires a gD receptor but not necessarily heparan sulfate. Virology 279:313-324.

67. Zhang J, Yang J, Jang R, Zhang Y. 2015. GPCR-I-TASSER: A Hybrid Approach to G Protein-Coupled Receptor Structure Modeling and the Application to the Human Genome. Structure 23:1538-1549.

68. Magrane M, UniProt C. 2011. UniProt Knowledgebase: a hub of integrated protein data. Database (Oxford) 2011:bar009.

69. Kondo N, Miyauchi K, Matsuda Z. 2011. Monitoring viral-mediated membrane fusion using fluorescent reporter methods. Curr Protoc Cell Biol Chapter 26:Unit 26 9.

70. Aldaz-Carroll L, Whitbeck JC, Ponce de Leon M, Lou H, Hirao L, Isaacs SN, Moss B, Eisenberg RJ, Cohen GH. 2005. Epitope-mapping studies define two major neutralization sites on the vaccinia virus extracellular enveloped virus glycoprotein B5R. J Virol 79:6260-71.

71. Connolly SA, Whitbeck JJ, Rux AH, Krummenacher C, van Drunen Littel-van den Hurk S, Cohen GH, Eisenberg RJ. 2001. Glycoprotein D homologs in herpes simplex virus type 1, pseudorabies virus, and bovine herpes virus type 1 bind directly to human HveC(nectin-1) with different affinities. Virology 280:7-18.

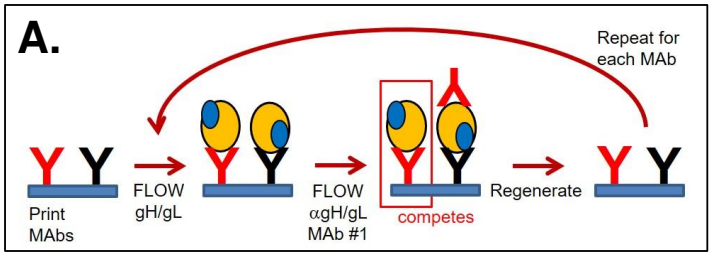

B. Heatmap for gH1/gL1

	BBH5	52S	46S	CHL37	CHL21	BBH3	53S	CHL27	L4	CHL30	CHL29	H6	BBH4	BBH2	LP11
BBH5		0.05	0.14	0.13	0.08	0.06	0.56	0.54	0.22	0.11	-0.01	0.05	0.32	0.30	0.68
52S	0.14		0.09			0.16	0.93		0.23	0.79	0.18	0.35	0.54	0.55	0.66
CHL37	0.10	-0.05	-0.13		0.11	0.22	0.76	0.33	0.23	0.17	0.16	0.24	0.54	0.53	0.75
CHL21	0.04	-0.10	-0.18	0.06		0.19	0.72	0.27	0.20	0.08	0.06	0.13	0.54	0.53	0.73
53S	0.56	0.90	0.99	0.61	0.64	0.25		-0.01	0.40	0.33	0.32	0.40	0.75	0.77	0.07
L4	0.24	0.56	0.40	0.37	0.27	0.16	0.57	0.23		0.15	0.16	0.29	0.34	0.35	0.46
H6	0.10	0.30	0.26	0.14	0.14	0.08	0.12	0.18	0.13	0.26	0.31		0.08	0.09	0.08
BBH4	0.42	0.79	0.71	0.51	0.49	0.24	0.78	0.24	0.25	0.07	0.04	0.13		0.09	0.04
BBH2	0.35	0.75	0.77	0.55	0.50	0.19	0.71	0.29	0.25	0.07	0.06	0.09	0.03		0.05
LP11	0.40	0.73	0.75	0.48	0.48	0.23	0.26	0.20	0.25	0.12	0.11	0.13	0.08	0.07	

C. Combined dendogram for gH1/gL1

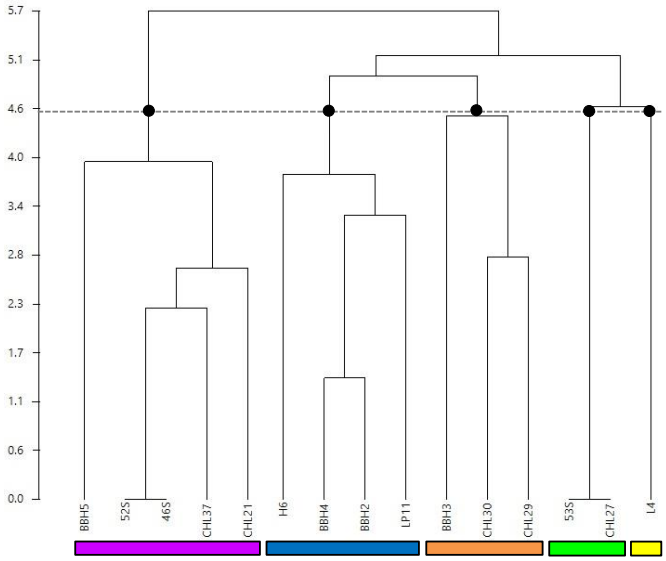

D. Heatmap for gH2/gL2

	CHL37	CHL21	CHL35	CHL31	CHL17	CHL29	CHL32	CHL30	53S	CHL27	CHL15	CHL9	CHL7	CHL14	CHL5	CHL11	CHL8	CHL12	CHL2	CHL16	CHL13	CHL10	CHL6	CHL4
CHL37		-0.02	0.12	0.12	0.26	0.26	0.37	0.21	0.28	0.07	0.22	0.44	0.23	0.42	0.37	0.42	0.44	0.26	0.31	0.39	0.40	0.45	0.29	0.34
CHL21	-0.01		0.14	0.12	0.27	0.22	0.38	0.16	0.29	0.10	0.24	0.44	0.24	0.42	0.36	0.43	0.44	0.27	0.33	0.40	0.40	0.44	0.31	0.36
CHL35	0.13	0.12		0.08	0.46	0.42	0.61	0.24	0.46	0.24	0.25	0.53	0.24	0.41	0.50	0.42	0.52	0.21	0.24	0.38	0.40	0.62	0.43	0.45
CHL18	0.38	0.56	0.31	0.28	0.34	0.21	0.44	0.30	0.25	0.24	0.27	0.51	0.23	0.32	0.34	0.30	0.32	0.27	0.31	0.12	0.16	0.16	0.20	0.34
53S	0.75	0.74	0.31	0.21	0.33	0.60	0.73	0.47		0.01	0.20	0.39	0.23	0.34	0.36	0.38	0.39	0.23	0.31	0.35	0.35	0.42	0.31	0.34
CΔ48L3	0.37	0.49	0.23	0.17	0.30	0.45	0.54	0.37	0.07	-0.04	0.05	0.27	0.11	0.19	0.22	0.23	0.25	0.11	0.19	0.17	0.19	0.26	0.17	0.21
CHL15	0.65	0.67	0.23	0.17	0.31	0.32	0.46	0.28	0.28	0.09		0.01	0.01	0.00	0.00	0.00	0.00	0.01	0.00	-0.01	0.00	0.00	0.00	0.00
CHL3	0.65	0.67	0.21	0.14	0.30	0.28	0.44	0.22	0.30	0.12	-0.03		0.00	0.00	-0.04	0.00	-0.02	0.00	0.02	0.00	0.00	0.00	0.03	0.00
CHL7	0.67	0.65	0.20	0.15	0.30	0.25	0.44	0.25	0.30	0.10	-0.01	-0.01		0.00	-0.01	-0.01	0.00	0.01	-0.03	0.00	0.02	0.01	0.02	0.01
CHL14	0.60	0.64	0.20	0.13	0.29	0.26	0.43	0.24	0.26	0.07	-0.03	-0.02	-0.03		-0.05	-0.06	-0.04	-0.02	-0.04	-0.04	-0.03	-0.05	-0.03	-0.04
CHL5	0.66	0.65	0.21	0.15	0.29	0.28	0.45	0.24	0.28	0.10	0.01	0.01	0.01	0.01		0.00	0.00	0.02	0.02	0.01	0.01	0.01	0.03	0.01
CHL11	0.64	0.67	0.22	0.14	0.30	0.27	0.41	0.22	0.30	0.12	0.00	0.00	0.01	0.00	-0.02		0.00	0.01	-0.04	-0.01	-0.02	-0.01	0.01	0.00
CHL8	0.64	0.67	0.21	0.14	0.29	0.25	0.43	0.21	0.29	0.11	0.02	0.00	0.01	0.01	0.02	0.00		0.03	0.01	-0.02	-0.01	-0.02	-0.02	0.02
CHL12	0.63	0.68	0.21	0.11	0.30	0.26	0.45	0.21	0.31	0.12	0.01	0.02	0.01	0.01	0.00	0.01	0.01		0.03	0.00	0.02	0.02	0.03	0.01
CHL2	0.67	0.68	0.27	0.20	0.34	0.34	0.53	0.33	0.28	0.12	-0.01	-0.02	0.00	0.02	-0.04	0.00	0.00	0.02		-0.01	0.01	-0.01	-0.02	0.00
CHL16	0.61	0.66	0.20	0.14	0.28	0.25	0.40	0.23	0.27	0.09	0.01	0.00	0.01	0.00	0.00	-0.01	-0.01	0.01	-0.02		0.00	-0.02	0.00	-0.01
CHL13	0.63	0.67	0.22	0.15	0.30	0.25	0.43	0.23	0.30	0.11	-0.01	0.00	0.01	0.00	-0.01	-0.01	0.00	0.02	-0.02	-0.02		-0.01	0.00	0.00
CHL10	0.66	0.67	0.21	0.13	0.30	0.26	0.46	0.22	0.31	0.12	-0.01	0.01	0.01	-0.01	-0.01	0.00	0.00	0.00	-0.04	0.01	0.01		0.02	-0.01
CHL6	0.64	0.65	0.21	0.15	0.29	0.27	0.44	0.24	0.30	0.12	0.02	0.02	0.02	0.00	0.02	0.01	0.01	0.02	0.02	0.01	0.02	0.02		0.02
CHL4	0.63	0.66	0.22	0.17	0.30	0.29	0.44	0.27	0.30	0.12	0.02	0.01	0.01	0.00	0.00	0.00	0.01	0.03	-0.02	-0.01	0.00	0.00	0.01	

E. Combined dendogram for gH2/gL2

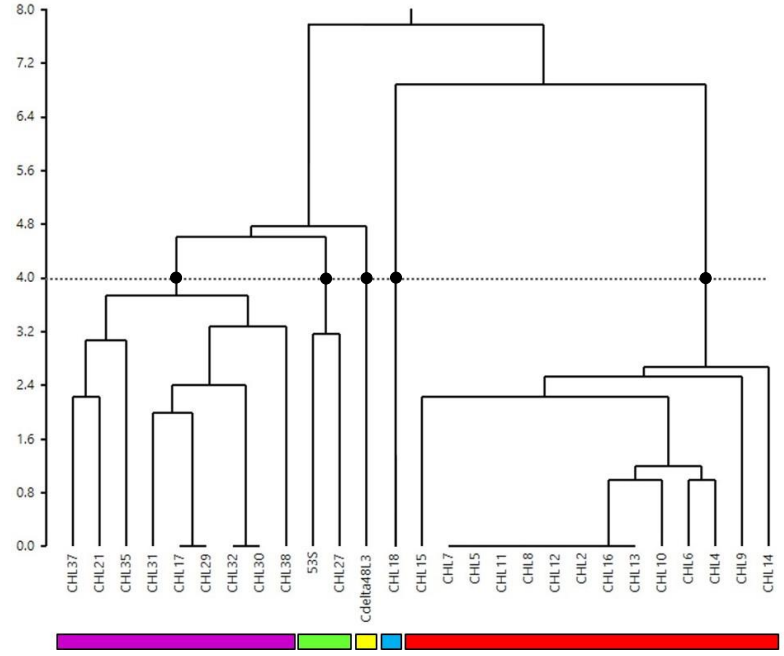

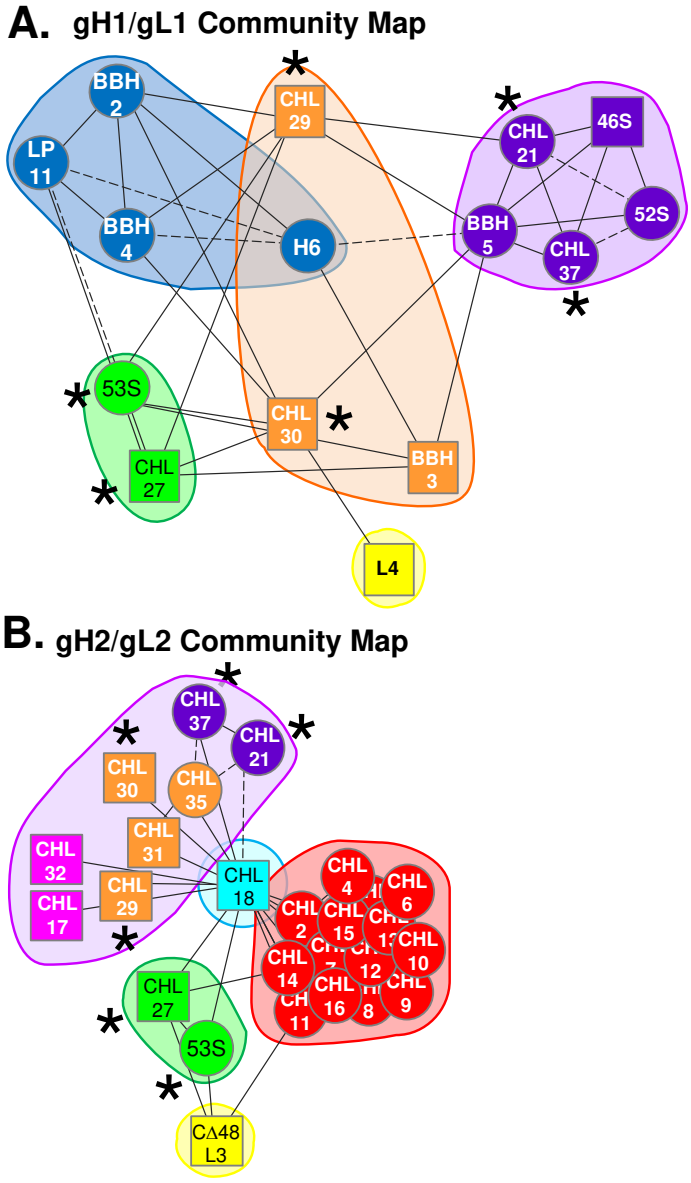

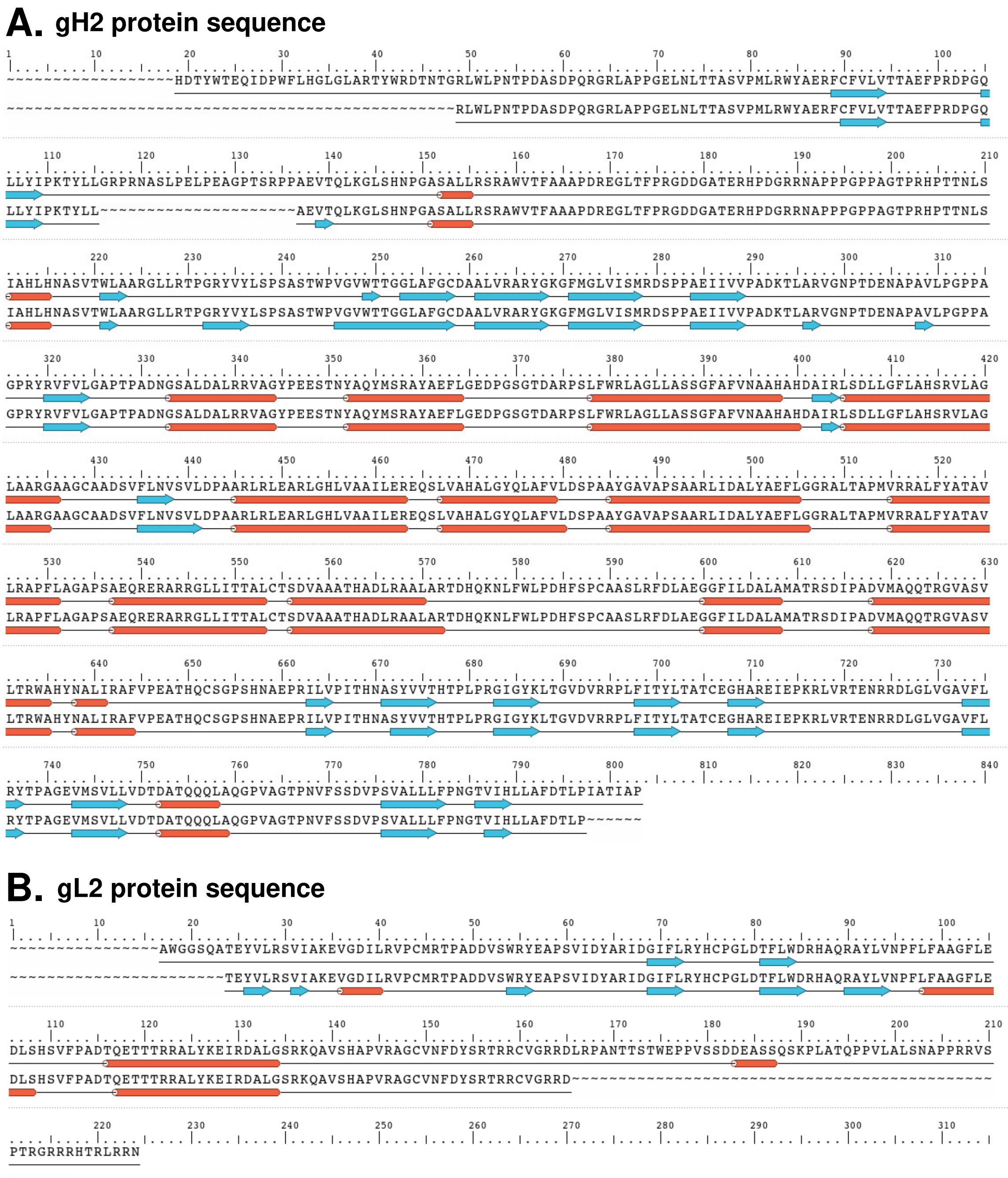

C. gH2/gL2 heterodimer, ribbon diagram

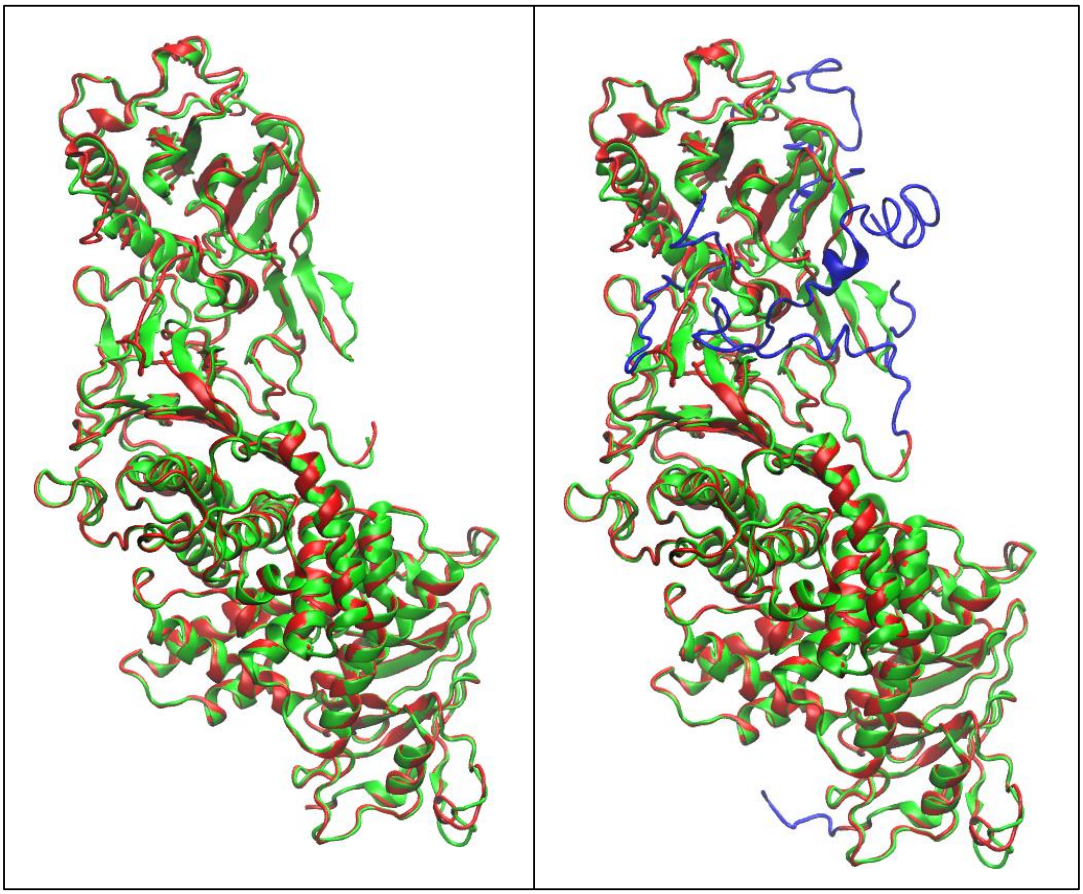

D. gH2/gL2 heterodimer, surface view

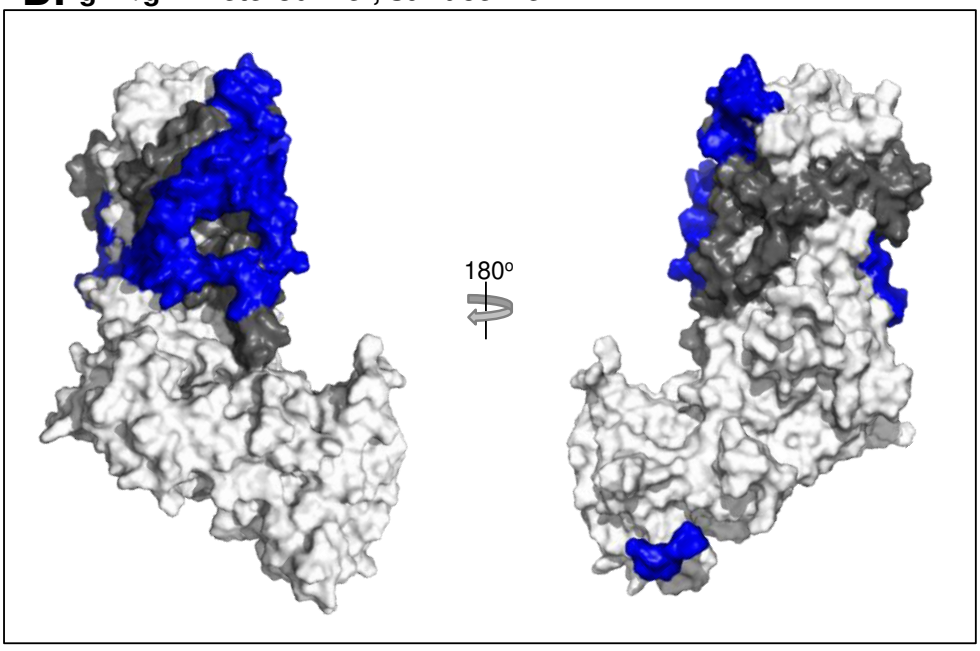

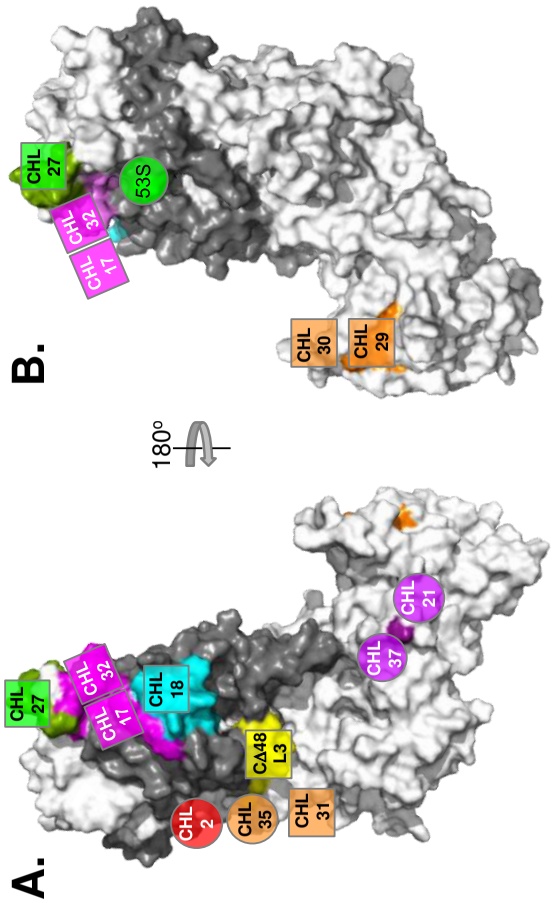

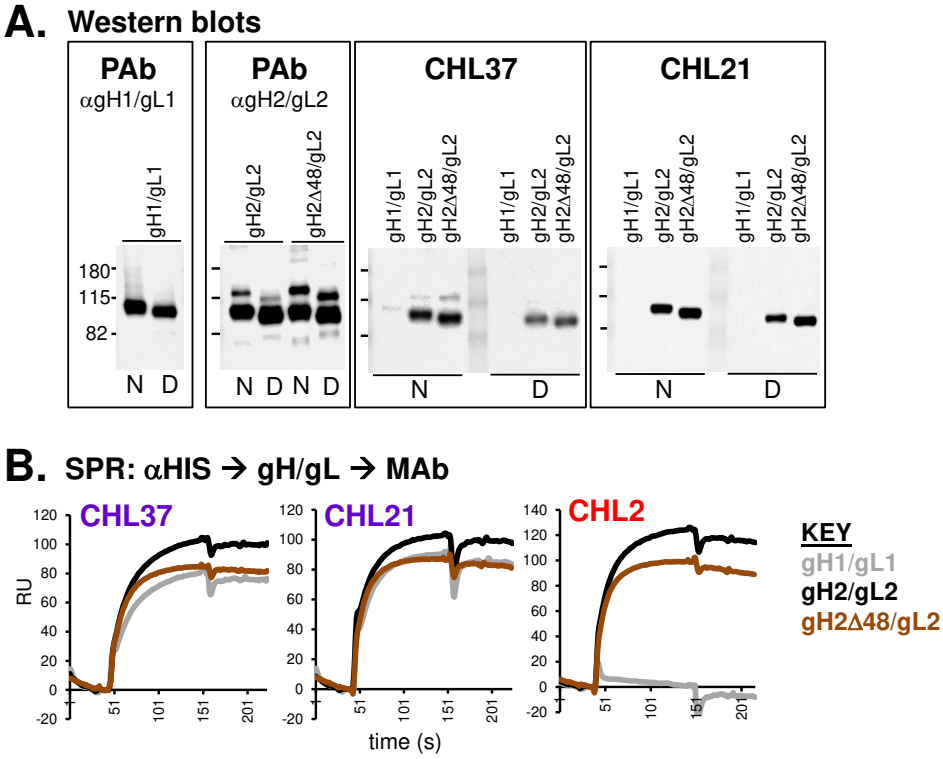

A. **SPR: αHIS → gH/gL → MAb**

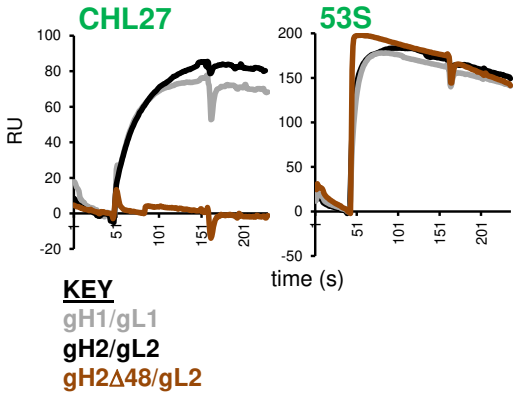

B. **Peptide ELISA** (CHL27)

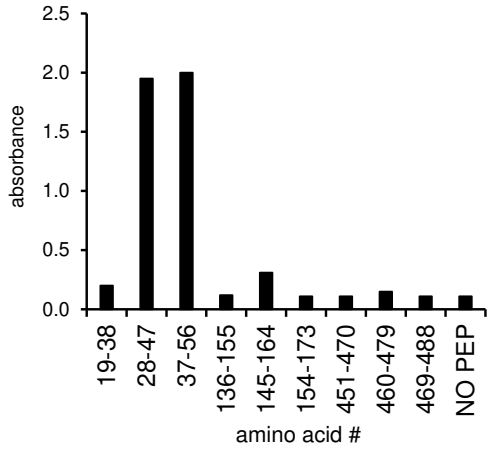

C.

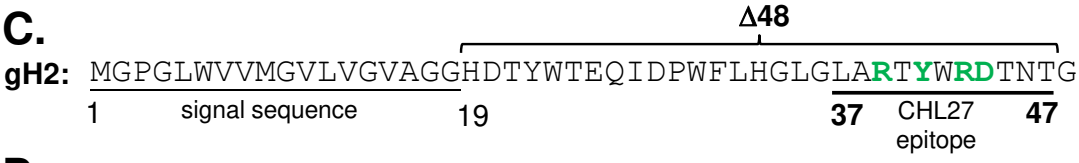

D. **Western blot**

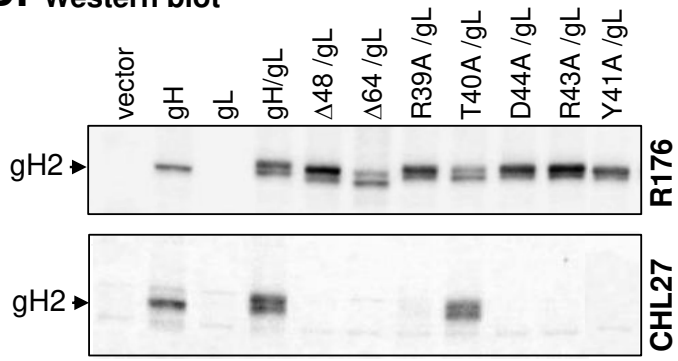

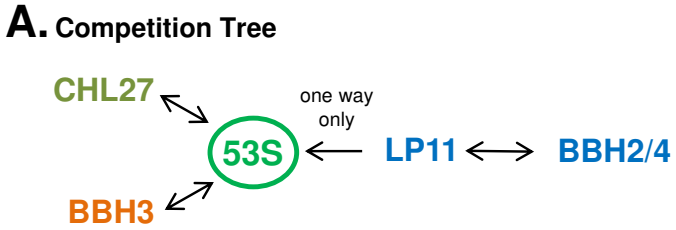

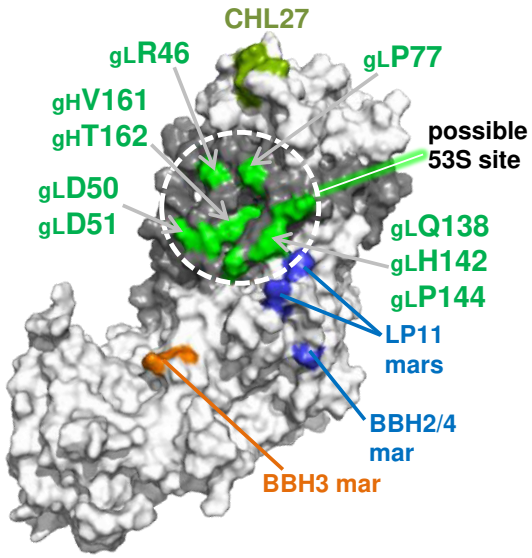

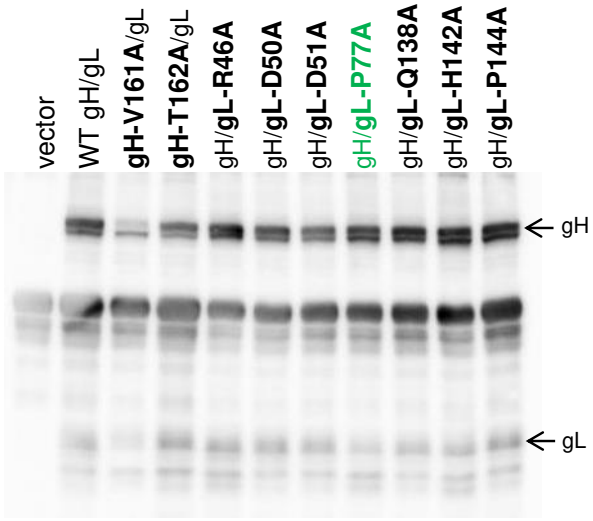

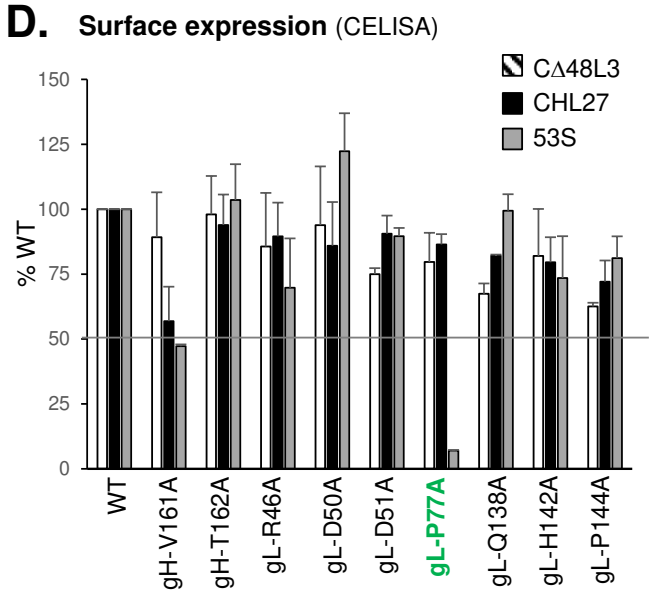

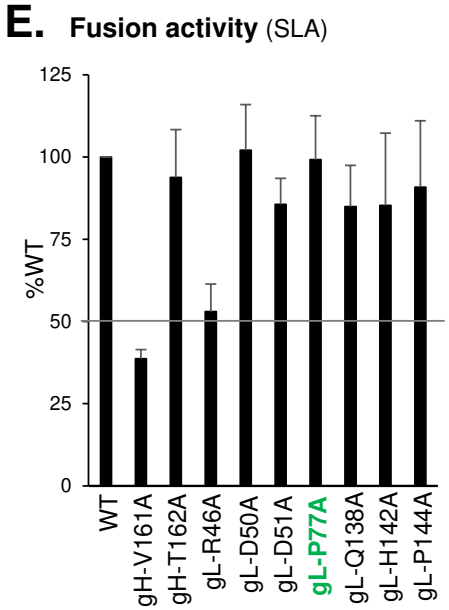

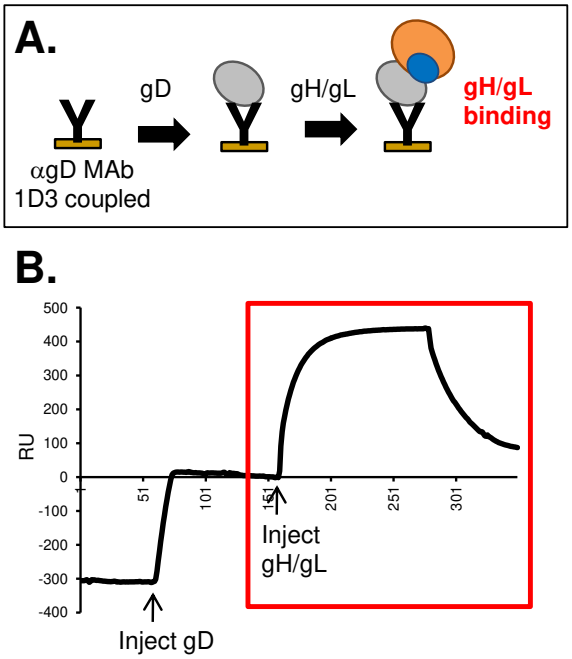

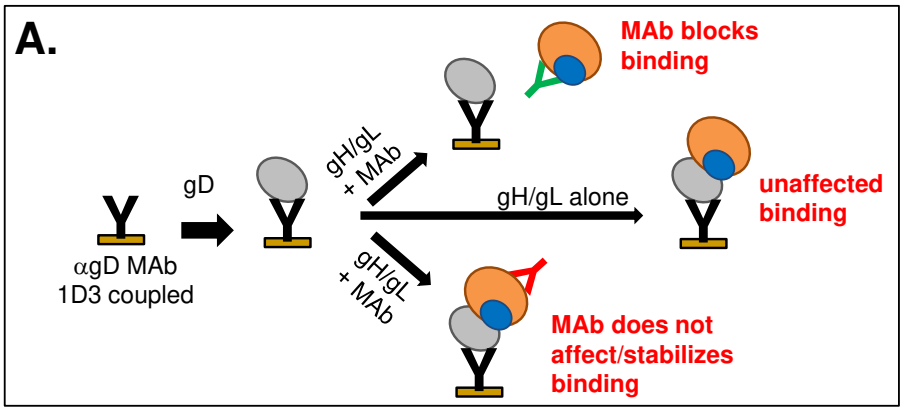

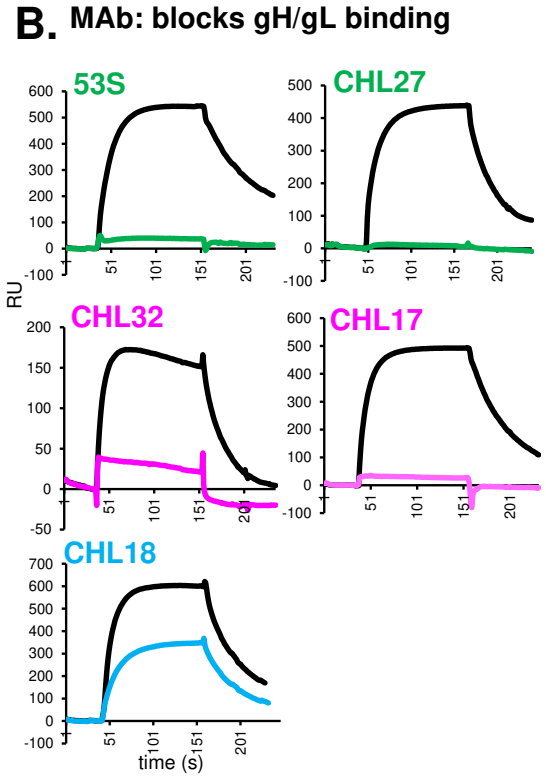

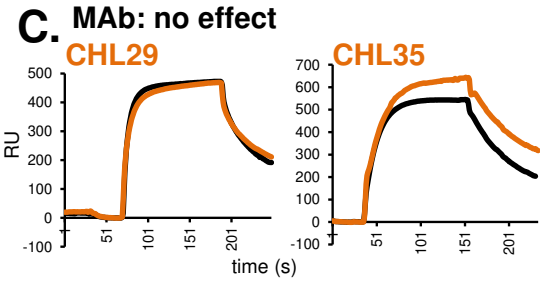

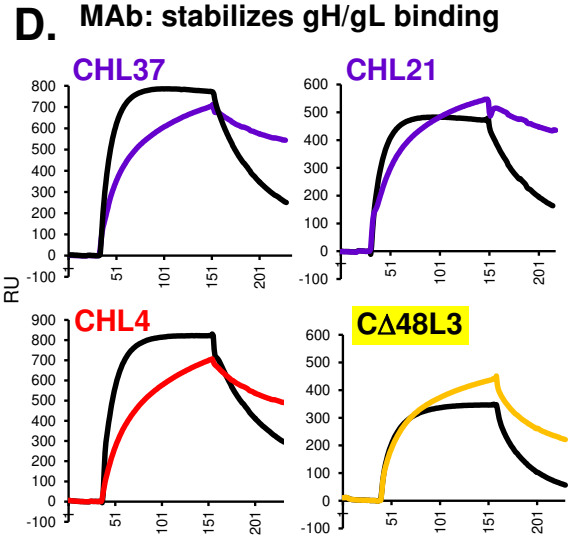

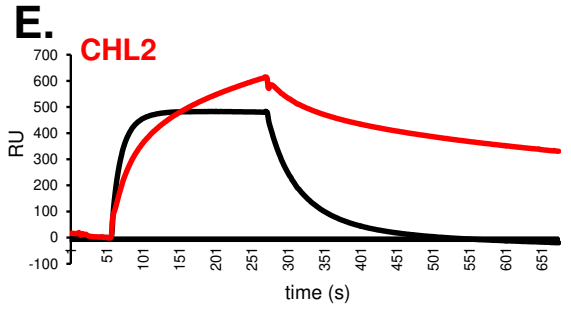

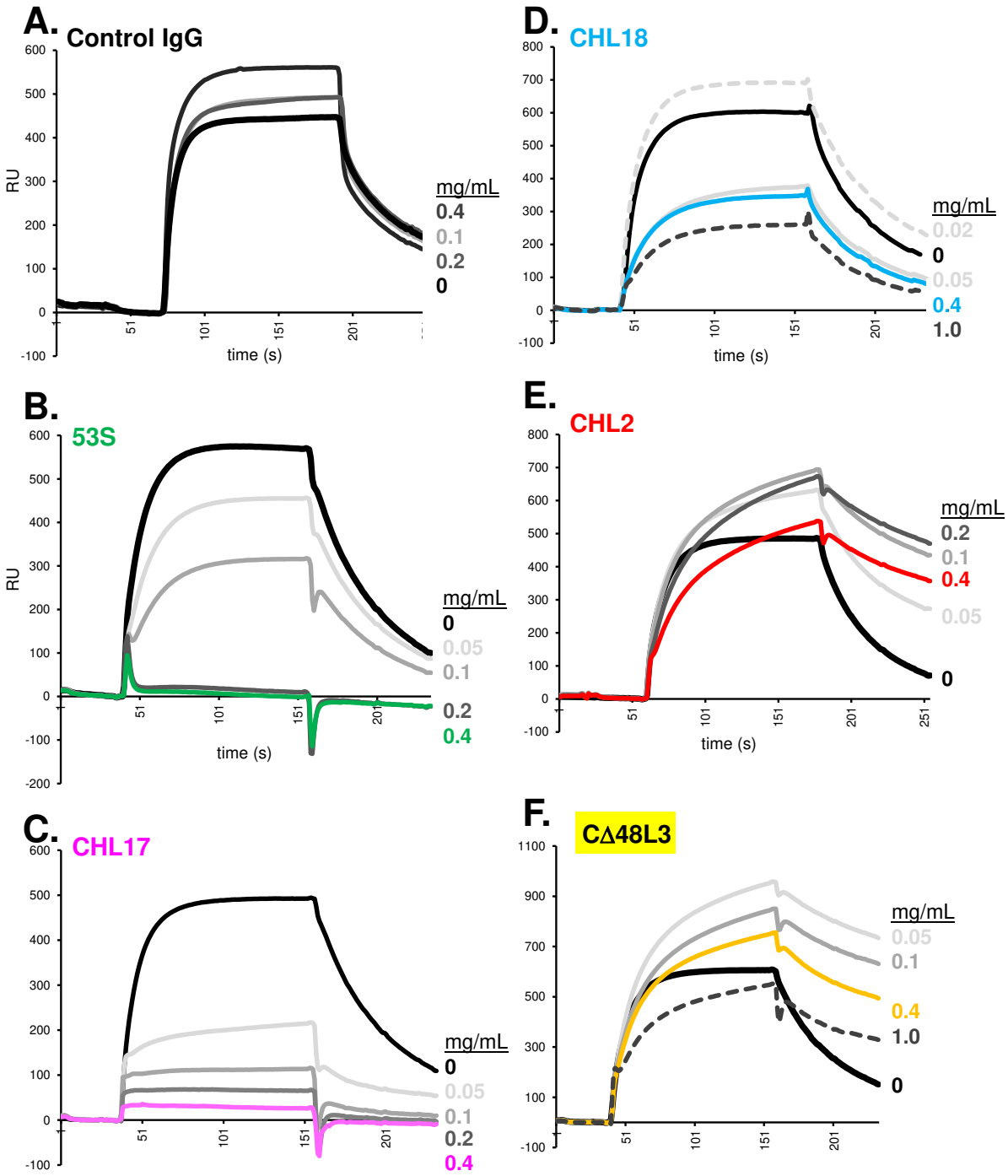

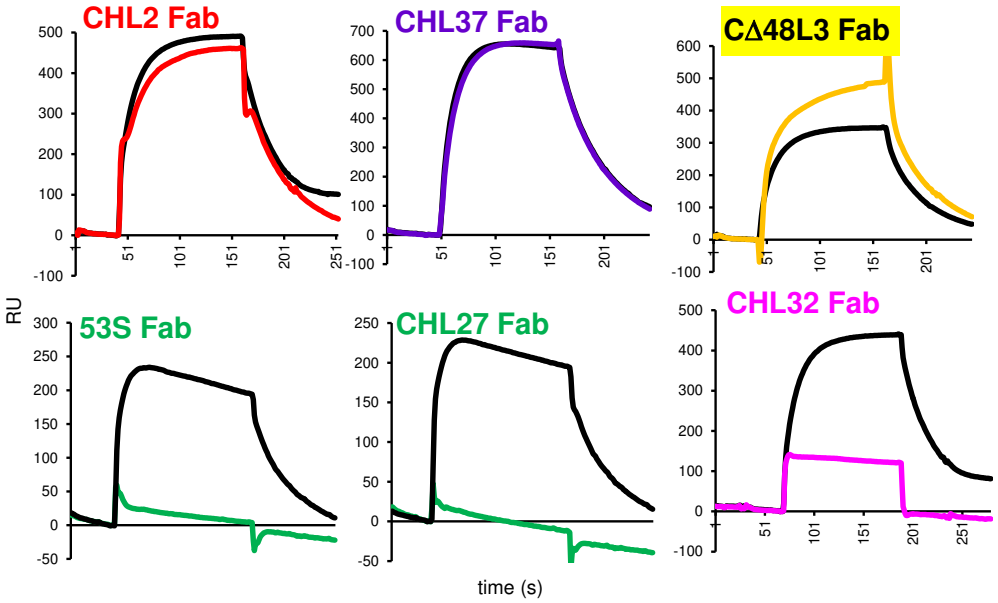

JVI Journal of Virology

Journal of Virology